Chapter 5
Numerical Modelling of Shelf Physical Dynamics

5.1 INTRODUCTION

Minimising negative impacts from offshore aquaculture is a key concern in coastal zone management for ensuring the sustainability of both the industry and the receiving environment. An in-depth understanding of shelf physical dynamics is a prerequisite for determining forcing mechanisms, subsequent responses, and interactions, thus allowing informed decision making prior to works approval and sustainable management of resources once they are established.

In the case of sustainable open coast aquaculture planning, a spatially comprehensive understanding of the workings and interactions of the hydrodynamics is essential. Numerical modelling provides the tools required (Henderson *et al.*, 2001).

Whilst instrument deployments have provided oceanographic data at targeted sites over the shelf, limitations with the number of instruments available coupled with the physical size of the Bay of Plenty shelf resulted in some uncertainty with respect to the spatial extent of observed dynamics. A calibrated numerical model of shelf dynamics offers reliable information over far greater spatial and temporal scales and resolutions than instrument deployments can provide. Numerical models enable the influences of a variety of forcing functions to be isolated and resolved. Further, they can drive ecological and water quality models and offer predictive capabilities. Even comprehensive instrument deployment arrays are unable to supply the necessary data to adequately fulfil these tasks, highlighting the need to develop a capable numerical representation of shelf dynamics.

5.2 MOTIVATION AND RELEVANCE TO THESIS OBJECTIVES

Achieving environmental sustainable aquaculture development requires a balance between the scale of development and the rate of production and supply of phytoplankton and nutrients along with waste dispersal rates (including localised depleted water masses, Pillay, 2004). The hydrodynamic regime is critical in regulating these factors. Indeed, several authors have observed strong positive correlations between cultured bivalve growth and current speeds (Frechette and Bourget, 1985; Emmerson, 1990; Pérez-Camacho *et al.*, 1995; Strohmeier *et al.*, 2005).

Developing a numerical representation of Bay of Plenty shelf hydrodynamics provides valuable information on the relative roles of mechanisms forcing the hydrodynamics

and provides key output required to determine ecosystem level impacts of potential developments through coupled ecological models. This modelling represents a significant step toward the goal of determining the potential for sustainable aquaculture within the region.

5.2.1 CHAPTER AIMS

This chapter aims to:

- calibrate a 3-dimensional numerical baroclinic model of shelf circulation within the Bay of Plenty, New Zealand.

To perform this task the influences and forcing mechanisms on shelf circulation must be identified, resolved, and numerically characterised. This leads to a further aim:

- to test key gaps in the current knowledge of Bay of Plenty shelf hydrodynamics as identified in the previous chapter by accurately resolving dominant influences on the Bay of Plenty shelf circulation, characterising those of significance, and including them in the final numerical model.

The physical, biotic, technical, and socio-economic setting in which a numerical model is applied often affects the modelling process and its subsequent application (Henderson *et al.*, 2001). It is essential therefore to have a clear understanding of the final applications of the model during the development phases. In this case, the calibrated model will subsequently be applied to:

- assist in the identification of a scale of suitability of the Bay of Plenty marine environment to suspended offshore aquaculture for planning purposes (Chapter 6);
- drive an ecological model predicting primary production and nutrient cycling characteristics within the Bay of Plenty (Chapter 7).

5.3 PARTITIONING INFLUENCES ON SHELF CURRENTS

Open coast shelf environments are recognised as being difficult to model due to the multitude of factors which may be responsible for forcing, influencing or modifying observed currents and sea-levels (Huyer, 1990; Huthnance, 1995; Csanady, 1997; Davies and Hall, 2002). Currents over and near continental shelves can be influenced by the presence of the coastal boundary, shelf geometry, wind and weather (local and remote), the locally specific tidal regime, the degree of stratification, the circulation of adjacent oceanic flows, and by any discharge of fresh water to the shelf (Huyer, 1990). To effectively replicate shelf flows in a numerical sense, each of these influences and their associated forcing mechanisms must be considered and addressed. Mechanisms driving these flows can include:

- tides;
- winds;
- buoyancy and density differences;

- oceanic forcing and boundary currents; and
- coastal trapped waves. (Csanady, 1997).

Each of these forcing mechanisms operates over characteristic (though variable) scales and frequencies. As noted in the previous chapter, there are key knowledge gaps related to some of these mechanisms influencing the Bay of Plenty shelf.

The consideration of each of these mechanisms represents a significant goal to the modelling exercise, especially given the present lack of information and paucity of oceanographic research in the area (*e.g.* de Lange *et al.* 2003). Detailed and judicious instrument deployments, data gathering and subsequent analyses, and targeted numerical modelling aid in the identification of the relative influences of each mechanism.

5.4 NUMERICAL MODEL DESCRIPTION

The 3DD numerical model (Black, 1995) is used to simulate both 2-dimensional currents, and 3-dimensional wind driven and buoyancy forced flows. This model has previously been successfully applied and calibrated within both New Zealand and international waters on numerous occasions since the 1980s (*e.g.* Black 1987, 1989; Black and Gay, 1987; Black *et al.* 1993, 2000; Middleton and Black 1994; Young *et al.* 1994; Hume *et al.*, 2000).

The 3DD model utilises an explicit finite difference (Eulerian) scheme to solve the momentum and continuity equations for velocity and sea level, through a series of vertical layers which are hydrodynamically linked by the vertical eddy viscosity. The model provides for spatial variation in roughness length (z_0) and horizontal eddy viscosity (A_H). Non-linear terms and Coriolis force can be included or neglected, while the land/sea boundaries can be set to free slip or no-slip.

The equations of horizontal motion for an incompressible fluid on a rotating earth in Cartesian coordinates with the z axes positive upward are:

$$\frac{\partial u}{\partial t}+u\frac{\partial u}{\partial x}+v\frac{\partial u}{\partial y}+w\frac{\partial u}{\partial z}-fv=-g\frac{\partial \varsigma}{\partial x}-\frac{1}{\rho}\frac{\partial P}{\partial x}+A_H\left(\frac{\partial^2 u}{\partial x^2}+\frac{\partial^2 u}{\partial y^2}\right)+\frac{\partial}{\partial z}\left(N_z\frac{\partial u}{\partial z}\right)$$

Equation 5.1

$$\frac{\partial v}{\partial t}+u\frac{\partial v}{\partial x}+v\frac{\partial v}{\partial y}+w\frac{\partial v}{\partial z}+fu=-g\frac{\partial \varsigma}{\partial y}-\frac{1}{\rho}\frac{\partial P}{\partial y}+A_H\left(\frac{\partial^2 v}{\partial x^2}+\frac{\partial^2 v}{\partial y^2}\right)+\frac{\partial}{\partial z}\left(N_z\frac{\partial v}{\partial z}\right)$$

Equation 5.2

$$w=-\frac{\partial}{\partial x}\int_{-h}^{z} u\,dz-\frac{\partial}{\partial y}\int_{-h}^{z} v\,dz$$

Equation 5.3

where t is the time, u and v are horizontal velocities in the x and y directions respectively, w the vertical velocity (positive upward), h the depth, g the gravitational

acceleration, ς the sea level above a horizontal datum, *f* the Coriolis parameter, *P* the pressure, A_H the horizontal eddy viscosity coefficient, N_Z the vertical eddy viscosity coefficient, and ρ is the density which varies with depth.

Assuming that vertical acceleration is neglected, the hydrostatic equation for the pressure at depth z is:

$$P = P_{atm} + g\int_z^{\varsigma} \rho dz \qquad \textbf{Equation 5.4}$$

where P_{atm} is the atmospheric pressure.

The physical representations of each of the various terms in the momentum equation are: local acceleration; inertia; Coriolis; pressure gradient due to sea level variation; pressure gradient due to atmospheric pressure; horizontal eddy viscosity; wind stress and bed friction. A_H varies spatially but the gradients are assumed to be small.

The salt and heat balance component of the model is coupled to the hydrodynamics through the application of a baroclinic pressure gradient associated with the horizontal temperature and/or salinity density field. The advection/diffusion equations are solved on the same grid as the hydrodynamics using a second-order-accurate, explicit, finite difference solution. The conservation equations for temperature and salinity may be written as:

$$\frac{\partial T}{\partial t} + u\frac{\partial T}{\partial x} + v\frac{\partial T}{\partial y} + w\frac{\partial T}{\partial z} = \frac{\partial}{\partial z}\left(K_z \frac{\partial T}{\partial z}\right) + K_H\left(\frac{\partial^2 T}{\partial x^2} + \frac{\partial^2 T}{\partial y^2}\right) \qquad \textbf{Equation 5.5}$$

$$\frac{\partial S}{\partial t} + u\frac{\partial S}{\partial x} + v\frac{\partial S}{\partial y} + w\frac{\partial S}{\partial z} = \frac{\partial}{\partial z}\left(K_z \frac{\partial S}{\partial z}\right) + K_H\left(\frac{\partial^2 S}{\partial x^2} + \frac{\partial^2 S}{\partial y^2}\right) \qquad \textbf{Equation 5.6}$$

where *T* is temperature, *S* is salinity, and K_H, K_Z are the horizontal and vertical coefficients of eddy diffusivity.

The density is computed according to an equation of state of the form,

$$\rho = \rho(T, S, z) \qquad \textbf{Equation 5.7}$$

The boundary conditions at the free surface z = ς are:

$$N_Z\frac{\partial u}{\partial z} = \tau_x^s \qquad N_Z\frac{\partial v}{\partial z} = \tau_y^s \qquad \frac{\partial \varsigma}{\partial t} + u\frac{\partial \varsigma}{\partial x} + v\frac{\partial \varsigma}{\partial y} = w^s \qquad \textbf{Equation 5.8}$$

where τ_x^s, τ_y^s denotes the components of wind stress , w^s is the vertical velocity at the surface, and

$$\tau_x^s = \rho_a \gamma\ |W|\frac{W_x}{\rho} \qquad \tau_y^s = \rho_a \gamma\ |W|\frac{W_y}{\rho} \qquad \textbf{Equation 5.9}$$

ρ is the water density, W the wind speed at 10 m above sea level while W_x and W_y are the x and y components, γ is the wind drag coefficient, ρ_a the density of air. The wind drag coefficient comes from the work of Wu (1982) where the drag coefficient γ is of the form,

$$\gamma = (0.8 + 0.065W_s) \times 10^{-3} \qquad \textbf{Equation 5.10}$$

where W_s is the numerical value in m.s^{-1} of the wind speed at 10 m above sea-level. Surface boundary conditions for salinity S_1 and temperature T_1 are,

$$N_z \frac{\partial S}{\partial z} = S_1 \qquad N_z \frac{\partial T}{\partial z} = T_1 \qquad \textbf{Equation 5.11}$$

where,

$$S_1 = \frac{S_0(E_1 - P_1)}{\rho} \text{ and } T_1 = \frac{Q}{c} \qquad \textbf{Equation 5.12}$$

and S_o is the surface salinity, E_1 is the net evaporation, P_1 is the net precipitation mass flux of fresh water, Q is the net ocean heat flux and c is the water heat capacity.

Assuming seabed slope is small, at the sea bed, $z = -h$, we have

$$N_z \frac{\partial u}{\partial z} = \tau_x^h \qquad N_z \frac{\partial v}{\partial z} = \tau_y^h \qquad \textbf{Equation 5.13}$$

where τ_x^h, τ_y^h denotes the components of bottom stress. Applying a quadratic law at the sea bed,

$$\tau_x^h = \mathrm{g}\, u_\mathrm{h} \left(u_h^2 + v_\mathrm{h}^2\right)^{1/2} / C^2 \qquad \textbf{Equation 5.14}$$

$$\tau_y^h = \mathrm{g}\, v_\mathrm{h} \left(u_h^2 + v_\mathrm{h}^2\right)^{1/2} / C^2 \qquad \textbf{Equation 5.15}$$

with u_h, v_h being the bottom currents and C is Chezy's C. For a logarithmic profile,

$$\mathrm{C} = 18 \log_{10}(0.37\, \mathrm{h}/z_o) \qquad \textbf{Equation 5.16}$$

where z_o is the roughness length.

The equation of state in a salinity-stratified condition can be approximated as,

$$\rho = \rho_0 + \alpha S \qquad \textbf{Equation 5.17}$$

where α is 0.74 at 20^{o}C and ρ_0 is the density of freshwater (1000 kg.m^{-3}).

The equation of state in a temperature and salinity stratified condition can be approximated as

$$\rho = 1000\ (1.0 - 3.7\text{x}10^{-6}\, T^2 + 8.13\text{x}10^{-4} S\ ) \qquad \textbf{Equation 5.18}$$

where $T = T' + 2.7$ and T' is the temperature in ^{o}C, S is the salinity (typically 35 ppt).

To solve the equations by the finite difference method, a staggered finite difference grid is utilised similar to that applied by Leendertse and Liu (1975). The sea level replaces w in the top layer. The solution is found by time stepping with a second-

order-accurate explicit scheme and third-order approximations for the non-linear inertia terms.

For the 3-dimensional temperature-stratified simulations (Section 5.6), the vertical eddy viscosity is based on a mixing length and Richardson number formulation, as

$$l_m(z) = \kappa z\left(1 - \frac{z}{h}\right) \quad \text{and} \quad N_0(z) = l_m^2\left[\left(\frac{\partial u}{\partial z}\right)^2 + \left(\frac{\partial v}{\partial z}\right)^2\right]^{1/2} \qquad \textbf{Equation 5.19}$$

where $N_0(z)$ is either the eddy viscosity N_z or eddy diffusivity K_z at elevation z above the sea bed, l_m is the mixing length, and κ is the Von Karman constant set to 0.4. In stratified flows, the gradient Richardson number is,

$$R_i(z) = \left(g\left(\frac{\partial \rho}{\partial z}\right)^2 / \left(\frac{\partial u}{\partial z}\right)^2\right) \qquad \textbf{Equation 5.20}$$

To determine the reduced vertical eddy viscosity in stratified flows, we use the Perrels and Karelse (1982) formula,

$$N_{(z)} = N_{0(z)} e^{-\alpha R_i(z)} \qquad \textbf{Equation 5.21}$$

$$K_{(z)} = K_{0(z)} e^{-\alpha R_i(z)} \qquad \textbf{Equation 5.22}$$

where $\alpha = 4$ for the eddy viscosity.

A Z-coordinate system is favoured over sigma co-ordinates to eliminate problems encountered when representing horizontal density gradients in a grid with non-horizontal grid cells. Similarly at the seabed, layered models typically represent a sloping seabed by a series of steps, with approximate heights equal to the model's vertical grid size. In baroclinic simulations, this can create local upwelling at the step walls, which is an artefact of the model's vertical resolution. These local upwellings can penetrate through the water column, causing a pattern of false internal wave activity. In 3DD, the depth is reproduced accurately by allowing fractionated cell sizes at the bed, which are less than the vertical grid size. The merits of the scheme have been assessed by simulating the steep profile used by Lamb (1994) to examine soliton formation (Black *et al.*, 1995). With the fractionated depth scheme, the velocities on the steeply-rising 'continental shelf' varied smoothly in the model. Additional aspects of the model with some relevance to the Bay of Plenty region are described by Black *et al.* (2000) who consider the three-dimensional baroclinic circulation of the nearby Hauraki Gulf.

5.5 TWO-DIMENSIONAL NUMERICAL SIMULATION OF BAROTROPIC TIDAL DYNAMICS

5.5.1 MODEL DOMAIN AND BOUNDARY CONDITIONS

Tidal dynamics were simulated over a computational domain which covered the entire Bay of Plenty region, from the Coromandel Peninsula in the west to East Cape in the east (Figure 5.1). The model domain was based on a 1000 x 1000 m grid resolution and oriented north-south (j-direction, 106 km) and east-west (i-direction, 207 km, Figure 5.1). All offshore islands and previously identified reef systems within the area were included. The model origin is located at 2761000mE, 6345000mN (NZMG1949).

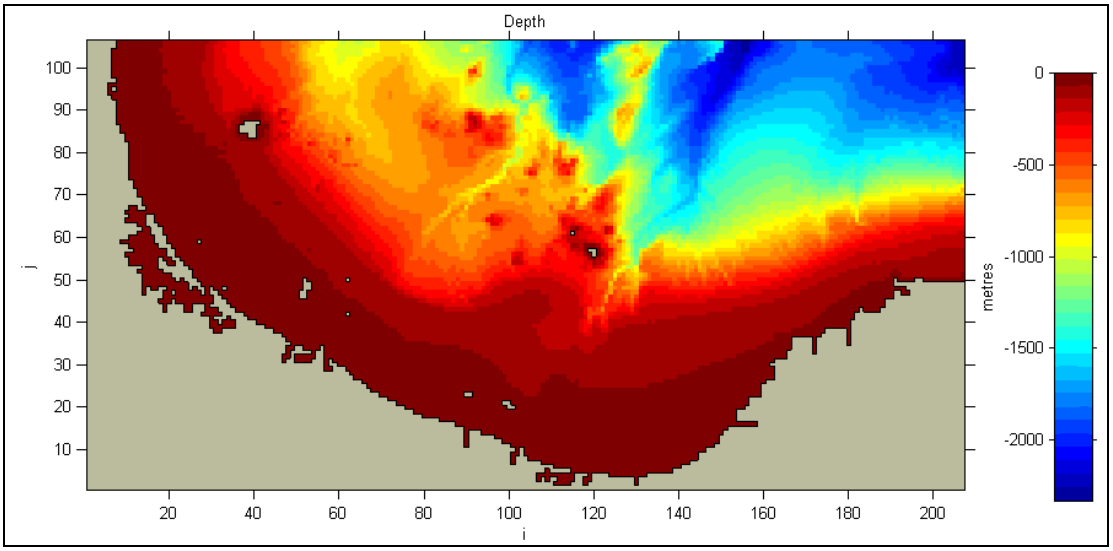

Figure 5.1 Model domain and bathymetry grid for 1000x1000 m grid used in the tidal modelling. The model grid, oriented north-south (j) and east-west (i), covers the region from the Coromandel Peninsula in the west to East Cape in the east. Model origin is located at 2761000mE, 6345000mN (NZMG1949).

Model bathymetry was interpolated to the 1000 m grid based on single-beam hydrographic sounding data from the local regional council. This database contains over 330,000 individual depth measurements (anomalous outliers removed) within the greater Bay of Plenty, with spatial data densities ranging from 1080 (oceanic regions) to 51100 (nearshore regions) measurements per model cell within the domain. Ascii text sounding files (latitude, longitude, depths) were converted to metric positions (New Zealand Map Grid 1949) and then interpolated to model bathymetry files using SURFER® software.

Model boundary conditions for the eastern and northern boundaries (Figure 5.1) were inferred from the Oregon state university Tidal Inversion Software (OTIS), an implementation of the global tidal model. OTIS is a package of programs for tidal data assimilation based on the methods of Egbert *et al.* (1994) and Egbert and Erofeeva (2002). OTIS applies a generalised inverse method, allowing the

combination of all the available information into global tidal fields, best fitting both the data and the dynamics in a least squares sense (Egbert and Erofeeva, 2002).

Water level fluctuations were adopted along the eastern model boundary and momentum fluxes along the northern boundary. Both boundary conditions were derived using all 10 available constituents from the world tidal model.

5.5.2 TIDAL MODEL CALIBRATION

Time-series of measured currents at Pukehina are long enough only to resolve the M_2, K_1 and O_1 constituents (Chapter 4), thus inhibiting the separation of the tidal currents using traditional harmonic analysis methodologies. As a result the tidal model was calibrated against water level elevations at Moturiki Island, the site of a long-term open-coast tide gauge (Figure 2.3). Moturiki Island is located well away from the model boundaries and near the coast, requiring the model to accurately transfer boundary information through the grid. Furthermore, the location requires that the model effectively deals with the dynamic interactions between water levels, currents, the bathymetry, and the coast.

Water levels recorded at Moturiki include oscillations due to tidal influences and also additional factors such as atmospheric conditions, wind set-up, pressure gradients etc. Analyses of these data with a tidal harmonic analysis program (T_TIDE, Pawlowicz *et al.*, 2002) resolves the signal into tidal and residual components. From the 730 day record of sea levels, 41 significant (95% level) constituents were resolved which explain 97.8% of the total variance. The tidal and residual components can then be used to validate the respective numerical hydrodynamic models.

Two parameters within the numerical model could be adjusted during the calibration stages; the friction coefficient (roughness length, z_o) and the eddy viscosity (A_H). During the runs the model was run for a period of ~3 months (210 M_2 cycles) to determine water level elevations and tidally induced current speeds at the Pukehina site.

The calibrated model replicates the observed measurements effectively and accurately (Figures 5.2 and 5.3). Values of z_o = 0.001 m and 100 m^2s^{-1} were applied as the friction coefficient (roughness length) and horizontal eddy viscosity respectively (Table 5.1). Constant values for both parameters were applied universally over the grid in the absence of alternative field data and the lack of sensitivity of the model to the coefficients.

Calibration runs revealed the model to be relatively insensitive to large changes in either friction coefficient or eddy viscosity magnitude, thought to be due to the relatively slow tidal current velocities (see Figure 5.6). The dominant influence was

the tidal boundary conditions, thus the results (Figures 5.2 and 5.3) demonstrate the accuracy of the world tidal model and boundary condition generation procedures.

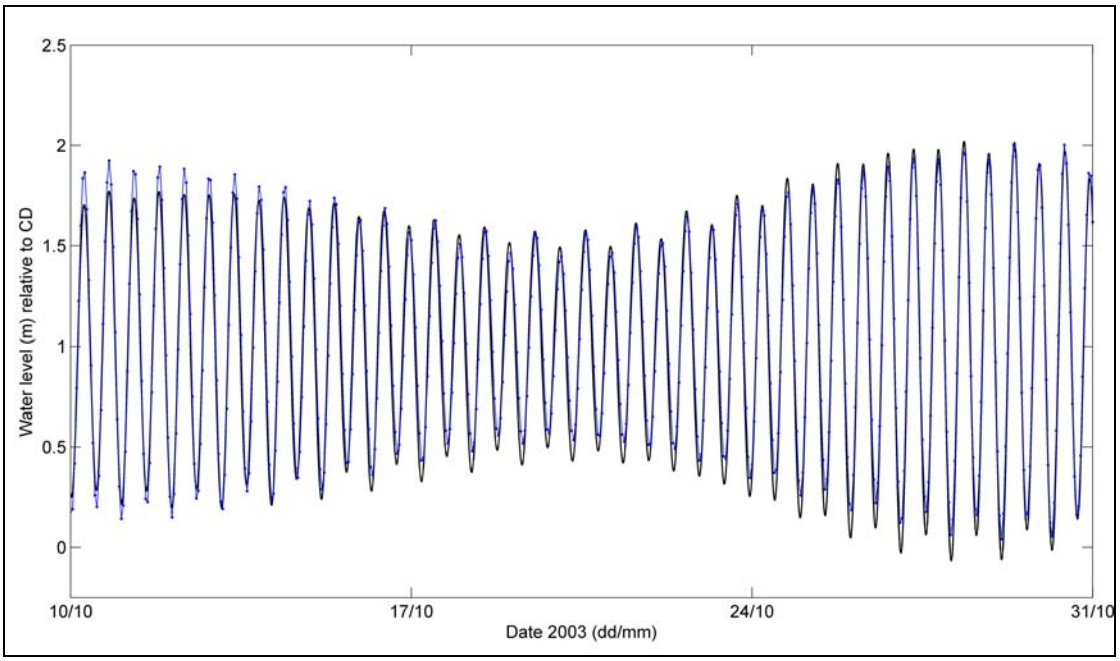

Figure 5.2 Tidal component of water levels observed at Moturiki (black solid line) and those predicted by the 3DD model (blue line with markers). Depths are relative to Moturiki datum.

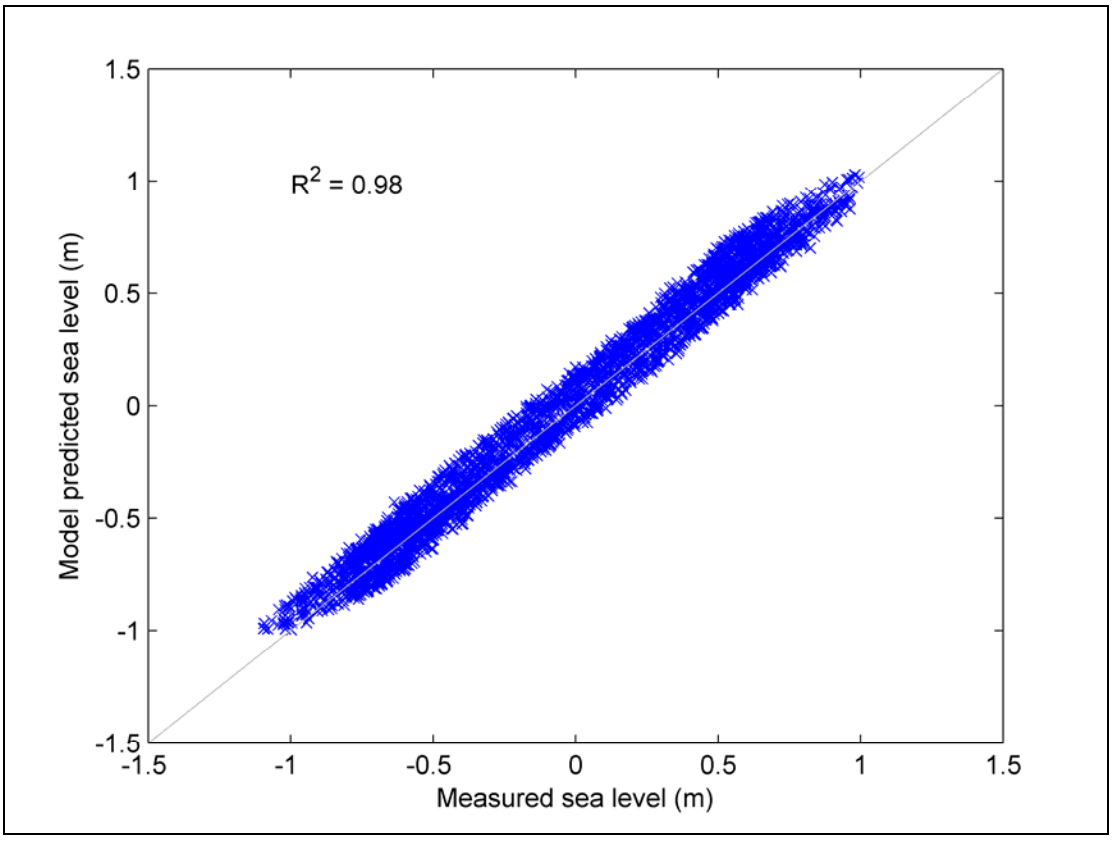

Figure 5.3 Scatterplot of observed and predicted water levels at Moturiki Island. Data points represent hourly measurements over 117 days (n = 2808).

Table 5.1 Numerical parameters for the two-dimensional barotropic tide model of the Bay of Plenty.

Parameter	Value
Time step	3 seconds
Roughness length	0.001 m
Horizontal eddy viscosity coef.	100 m^2s^{-1}
Model time start (t_0)	26/9/2003 0:00 NZST
Grid resolution	1000 m x 1000 m
Grid dimensions	207 x 106
Grid orientation	0^o true
Grid origin	276100 mE, 634500 mN, NZMG1949
Grid latitude (centre)	-37^o
Coastal slip	10%
Effective depth	0.3 m
Drying height	0.05 m
North boundary	OTIS flux values – world tidal model
East boundary	OTIS elevation values – world tidal model

5.5.3 TIDALLY FORCED CURRENTS WITHIN THE BAY OF PLENTY

Typical peak ebb and flood tide currents on the shelf ranged between 0.05 and 0.2 ms^{-1} (Figures 5.4, 5.5, and 5.6). Faster currents were predicted nearer tidal inlets and harbours. However, though sensible, these results (near inlets) should be treated with caution as the model is specifically targeted to shelf environments, with grid resolutions reflecting this, rather than toward smaller-scale features such as harbours and inlets.

Notably, modelled tidally driven velocity components are much smaller than velocities measured by the ADP (Figure 5.6). In addition, a progressive vector diagram of the ADP data including tides and with tides filtered out (Figure 5.7), indicates that tidal contributions to residual flow paths are negligible, except possibly at the tidal inlets. As non-tidal flows are substantially faster than the tidally forced flows (Figure 5.6) and the residual movement of the tidal component is negligible (Figure 5.7), it can be concluded that the dominant mechanism for flushing, mixing, and transmission of nutrients throughout the Bay of Plenty is the non-tidal circulation.

This general result is consistent with that found in Chapter 4, through harmonic analyses and low pass filtering the ADP record, and also with that of Sharples and Grieg (1998) from the shelf of the Hauraki Gulf.

As a result of these findings, the study now focuses on non-tidal currents and their prediction.

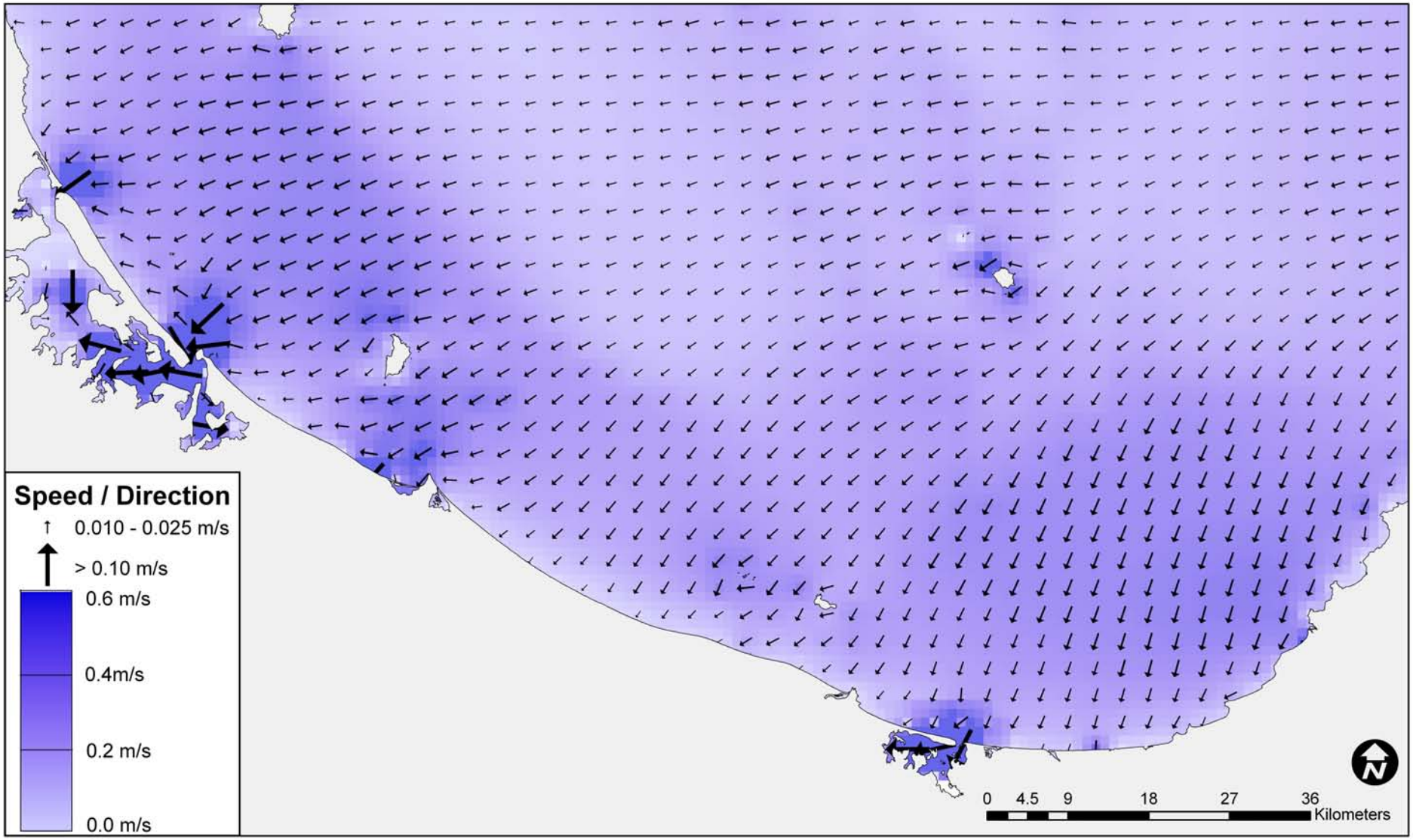

Figure 5.4 Tidally generated currents over the Bay of Plenty shelf during spring tides at mid flood stage.

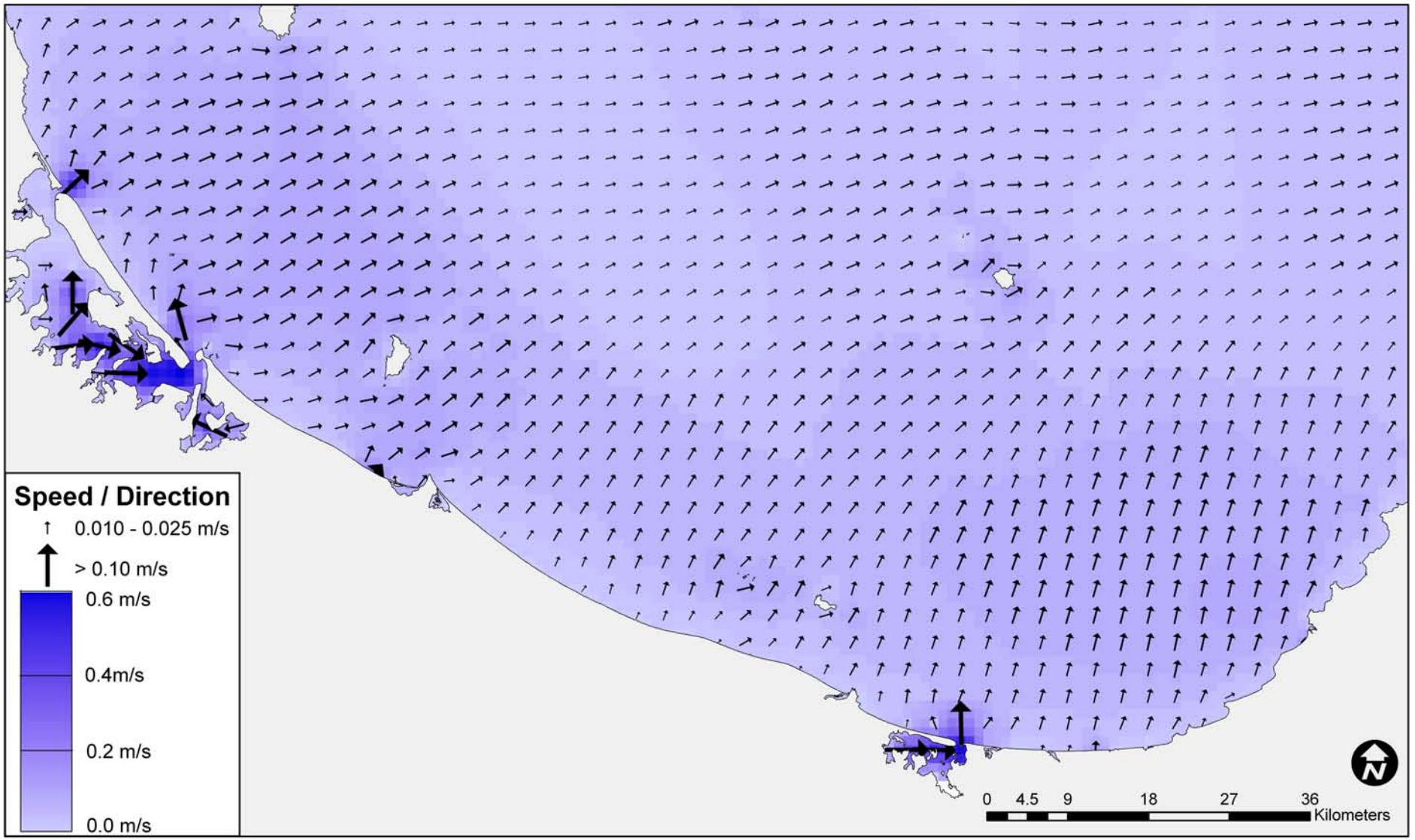

Figure 5.5 Tidally generated currents over the Bay of Plenty shelf during spring tides at mid ebb stage.

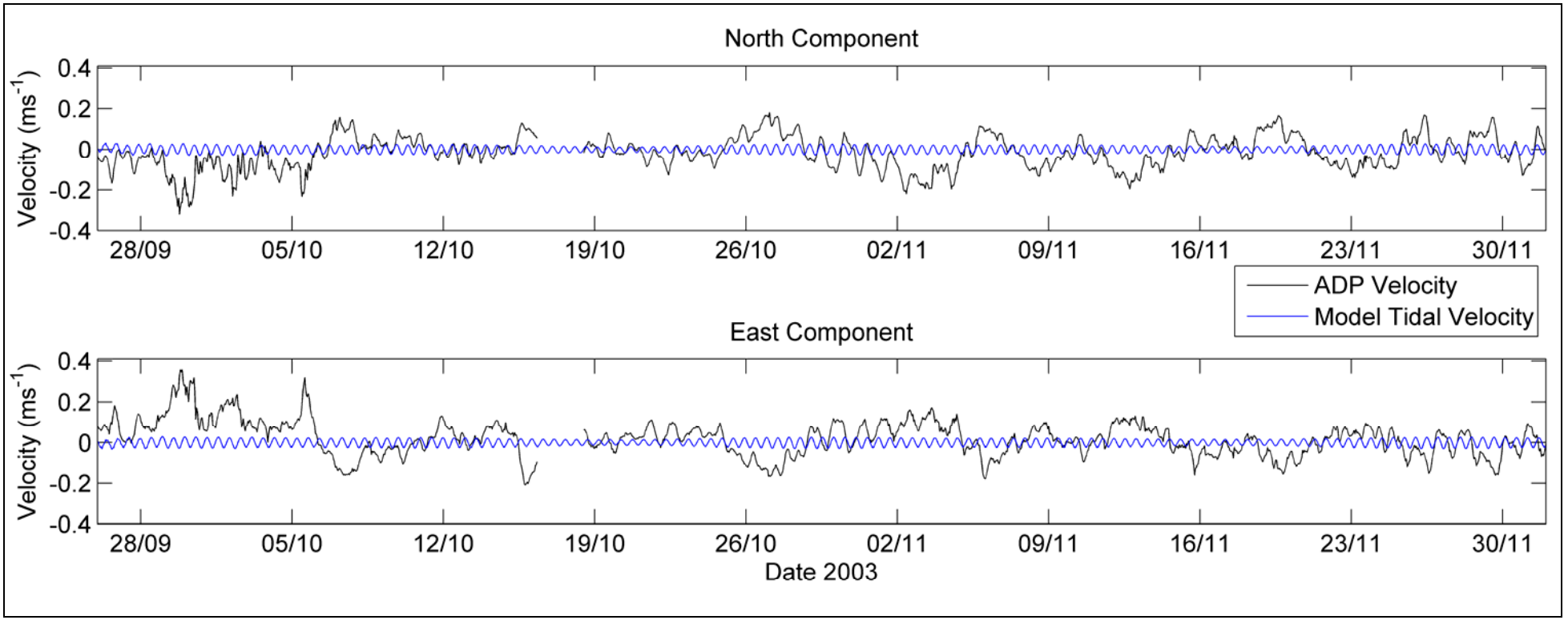

Figure 5.6 Depth averaged measured velocities (total currents) and depth averaged tidal flow components (from calibrated model). The ADP was serviced between 17 and 18/10/2003.

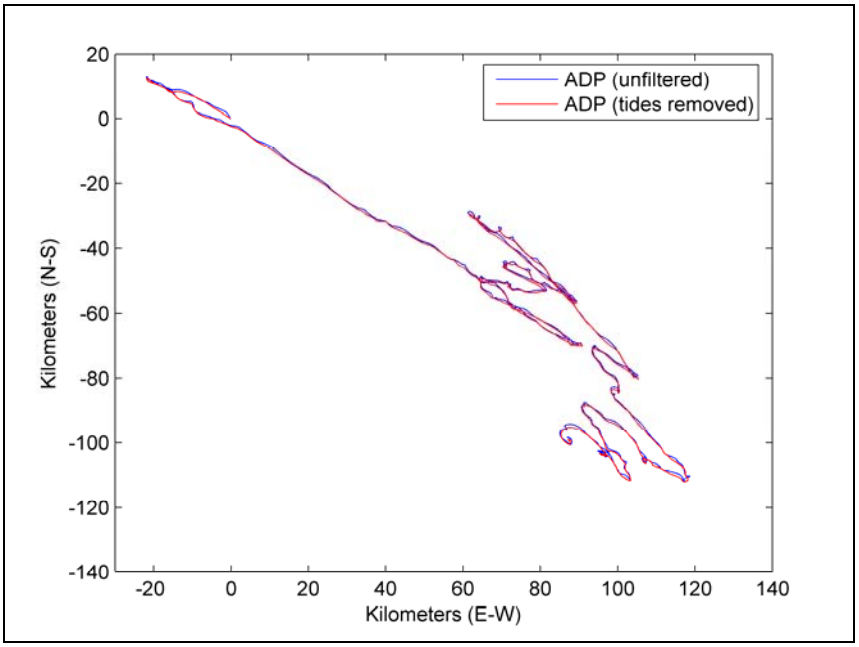

Figure 5.7 Progressive vector diagram of depth averaged ADP data including tides, and with the tidal component filtered out, at the Pukehina 65 m site. The consistency between the two progressive vectors indicates that the tidal component contributes little in terms of the residual net movement of the water column. Vectors have been placed 'nose on tail' over the period when the ADP was out of the water for servicing.

5.6 THREE-DIMENSIONAL, BAROCLINIC WIND DRIVEN DYNAMICS

A three-dimensional wind-driven baroclinic numerical model of the shelf region incorporates not only wind driven dynamics but also the influences of density driven flows and the effects of stratification within the water column. These models consider the dynamic wind shear stress on the ocean surface, internal shear stresses between model layers, bed friction, density driven flows, pressure gradients, geostrophic influences, and their interactions with the local topography and bathymetry in addition to solar heating and surface heat fluxes.

These models are typically highly complex through their requirement for multiple, time varying inputs (*e.g.* temperature and salinity profiles) over large spatial scales. Challenges include the establishment of initial conditions at the start of the model run (throughout each model depth layer) and the determination and numerical characterisation of boundary conditions specifying sea levels along with temperature and salinity profiles in all open boundary cells. Available boundary data is often sparse in both a temporal and spatial sense, which places a strong emphasis on rigorous calibration of the model output.

Baroclinic heat flux models have rarely been applied within New Zealand water bodies (*e.g.* Black *et al.* 2000) due to their complex nature; as such, this modelling is leading edge and demanding. The study area itself, being an open coast shelf environment is a particularly difficult location to apply such a model (Huyer, 1990; Huthnance, 1995; Csanady, 1997; Davies and Hall, 2002) and represents a further

challenge. Such a complex model is required for the current task for two main reasons, 1) instrument measurements have shown the shelf dynamics to feature highly 3-dimensional aspects *e.g.* upwellings on a shelf of variable width and significant density stratification, and 2) that the model will subsequently drive an ecological model of the shelf which must be in 3-dimensions to accurately represent the light, nutrient, and phyto-plankton/zoo-plankton structure of the shelf, all of which are highly variable with depth.

5.6.1 INITIAL CONDITIONS, BOUNDARY CONDITIONS AND INPUT FILES

5.6.1.1 MODEL DOMAIN AND DEPTH SCHEMATISATION

The computational domain of the three-dimensional baroclinic modelling was simplified somewhat relative to that used for the tidal modelling. The transition from a single layer two-dimensional model to a full three-dimensional schematisation with 10 depth layers increases the required computational effort several orders of magnitude. Furthermore, limitations of output data file size (2 GB with 32 bit software applications), resulted in the need to decrease the computational grid resolution to 3000 x 3000 m. Greater resolution surrounding proposed aquaculture farms could be achieved by nesting finer grids within the present model. Such techniques are beyond the scope of this thesis but could provide additional information at farm or inter-farm scales. This is especially true of the subsequent ecological model where a key weakness of the existing literature is poor replication of boundary conditions for farm scale models.

In order to maximise depth resolution within the available 10 layers, the bathymetry grid was truncated at 1000 m. The finalised model domain was oriented north-south (j-direction, 114 km) and east-west (i-direction, 207 km, Figure 5.8). All major offshore islands were retained in the schematisation. Model origin is located at 2761000mE, 6339000mN (NZMG1949).

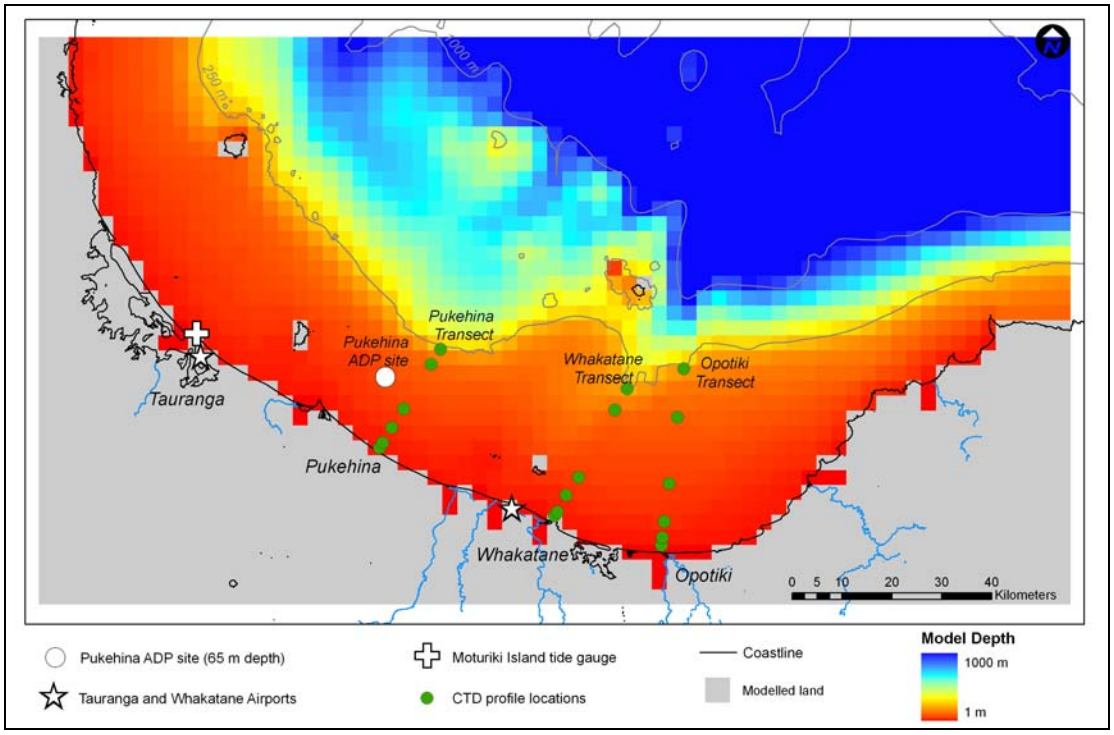

Figure 5.8 Model domain, bathymetry grid, and instrument locations for 3000x3000 m grid used for baroclinic wind driven modelling. The model grid, oriented north-south (j) and east-west (i), covers the region from the Coromandel Peninsula in the west to East Cape in the east. Model origin is located at 2761000 mE, 6339000 mN (NZMG1949). Note that the Tauranga Harbour has not been modelled as the 3 km resolution of the model grid renders predictions in this relatively small scale feature meaningless.

Model depth layers (Table 5.2) were selected based on temperature, salinity, and current profiles observed along the survey transects (Chapter 4). Model depth layer structure is most concentrated close to the surface where the greatest seasonal variation occurs (Figure 5.11). This consideration provides the model the best opportunity to replicate observed thermocline depths and water column structure.

Table 5.2 Structure of depth layers used in the three-dimensional numerical modelling within the Bay of Plenty.

Layer	Layer thickness (m)	Depth at base of layer (m)
1	5	5
2	10	15
3	10	25
4	10	35
5	15	50
6	20	70
7	80	150
8	100	250
9	250	500
10	500	1000

5.6.1.2 SEA LEVEL BOUNDARIES

Numerical models of shelf environments over such large spatial scales (207 km across the grid) require specific allowances for processes and dynamics acting over similar length scales (or greater).

Along-shelf winds combine with geostrophy to set up cross-shelf pressure gradients, reflected in cross-shelf sea level gradients (Csanady, 1981 and 1982; Bowden, 1983; Pond and Pickard, 1983). Additionally, this pressure gradient, again combined with geostrophy, leads to along-shelf currents in the same direction as the wind stress (Csanady, 1981; Smith, 1981). Dynamics leading to these conditions have been observed from ADP records within the Bay of Plenty (Chapter 4). Neglecting this effect at the open boundaries potentially leads to inaccurate prediction of the currents, especially near the land where the impact is more acute. However, it is difficult to forecast sea-level gradients as they are intimately linked to the magnitude of the currents, which are not known *a priori*.

A unique (to the 3DD model) 'Corioilis Boundary' is applied along the northern edge of the model domain to account for these effects. This boundary uses the predicted currents to back-calculate the pressure gradient along the boundary, and then applies this information directly back to the water levels as the model is running. The effect is a 'flapping' boundary which oscillates at the western end (landward edge) and is fixed at the eastern (oceanic edge). Sea levels across the eastern open boundary are fixed to 1.1 m above chart datum, corresponding to Mean Sea Level (MSL).

5.6.1.3 WIND FORCING

The two meteorological recording stations within the model domain, from which data are available, are Tauranga and Whakatane airports (Figure 5.8). Again however, due to the spatial scale of the model domain, two relatively nearby meteorological stations cannot be expected to accurately resolve the expected meso/synoptic-scale variations in wind strength and direction which can be observed across the model domain (Figure 5.9).

To best accommodate potential variability in wind vectors across the model domain, data inferred from the SeaWinds instrument onboard the QuikSCAT satellite were obtained throughout the Bay of Plenty between 2003 and 2005.

Comparison of QuikSCAT data from the node nearest Tauranga airport over a common year of measurement resulted in a reasonable correlation ($R^2 = 0.71$), with the QuikSCAT data overestimating the Tauranga wind stress ($\propto$ velocity^2) by a factor of 2.2 (Chapter 4).

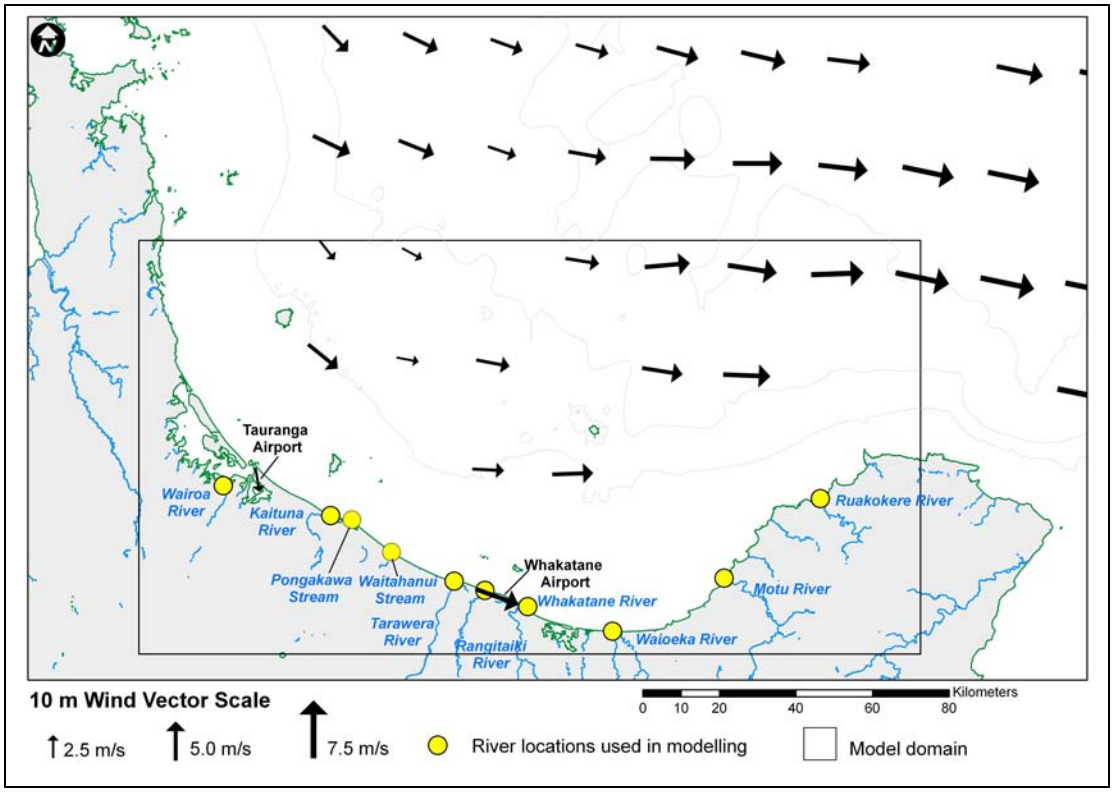

Figure 5.9 QuikSCAT, Tauranga, and Whakatane 10 m wind vectors at 1800 hrs, 22 June 2003. Note the variability in direction and magnitude of wind vectors across the model domain. Modelled river input points shown by yellow circles.

A total of 16 wind stations were used to define the wind field over the model grid for all runs, including 14 QuikSCAT nodes and both Tauranga and Whakatane stations.

5.6.1.4 ATMOSPHERIC PROPERTIES

Hourly time series of atmospheric properties including air temperature (^{o}C), barometric pressure (mbar), relative humidity (%), and solar radiance (Photosynthetically Active Radiation, PAR, Wm^{-2}) were obtained from both Tauranga and Whakatane airport stations. These data are required for the determination of hydrostatic pressure, wind stresses, and heat and salt balances within the model. Average cloud cover (not measured) was set to 0.45 and the albedo set to 0.08 which is within generally accepted limits (0.05 – 0.10, Pickard and Emery, 1990).

In practice, solar heating can be well modelled with two wavelength fractions, roughly corresponding to the blue/green (~390-577 nm) and yellow/red (~577 – 780 nm) wavelengths (though this division is somewhat arbitrary). This approach significantly reduces the complexity of representing all wavelengths separately while still representing the shape of the irradiance curve well, and is used throughout the literature (*e.g.* Manizza *et al.*, 2005)

Light decay constants, determining the penetration of incoming solar radiation into the water column were obtained by developing a 1-dimensional MATLAB® based model of surface heat fluxes and forecasting the measured stratification. ADP measured

currents enabled the determination of observed vertical shear and mixing, thereby narrowing the focus of the model to solely ocean/atmosphere heat fluxes. When calibrated against CTD data obtained co-incident with the ADP currents, the mean extinction coefficients across 10 sites were found to be: K_L = 0.574 (long-wave) and K_S = 0.128 (short-wave). The ratio of long to short-wavelengths in the measured solar radiation was taken to be 0.75, a standard value used within the 3DD model.

5.6.1.5 FRESHWATER INPUTS

Freshwater flow into the Bay of Plenty was replicated through the inclusion of 10 point source volume fluxes of low salinity water into the grid. Daily time series of flow volumes were obtained from the local regional council. Only rivers with mean flow volumes exceeding 10 m^3s^{-1} were included. Pongakawa and Waitahanui streams are exceptions however, and due to their close proximity to each other and cumulative flow volumes (> 10 m^3s^{-1}), were also included as point sources of fresh water. The rivers identified and modelled included (Figure 5.9):

- Wairoa River;
- Kaituna River;
- Pongakawa Stream;
- Waitahanui Stream;
- Tarawera River;
- Rangitaiki River;
- Whakatane River;
- Waioeka River;
- Motu River; and
- Ruakokere River.

Incoming freshwater was set to 0 ppt salinity and diluted into the calculated volume of salt water in the river mouth cell. No measured data were available for river water temperatures, so three-daily 1 km resolution AVHRR SST data (see Chapter 4 for description and validation) were used to interpolate a time series of water temperature at each river mouth for the duration of the modelling period. Incoming freshwater was assigned an inferred temperature profile based on these data.

5.6.1.6 TEMPERATURE AND SALINITY STRUCTURE

The three-dimensional baroclinic model requires the initial prescription of both temperature and salinity across the grid. In addition, a time series of each property at the open boundaries is required. Specialist software was developed to create the hot-start file specifying initial conditions at model start up along with the open boundary conditions.

5.6.1.6.1 INITIAL CONDITIONS

The CTD survey programme (Table 4.1 and Figures 4.1 and 4.2) provides essential data over the continental shelf (<200 m depths) to specify model initial conditions. The survey of 17 October 2003 is nearest to the model start time (22 days prior) making it the most relevant data on which to base initial modelled nearshore profiles of temperature and salinity. Observed data were averaged through each model layer to obtain indicative values at each profile site.

A lack of information regarding the water column structure farther offshore (depths > 200 m and >50 km from land) created a necessity to search for potential data sources (both historical and more current) describing the temperature and salinity structure of the oceanic waters off north-eastern New Zealand. The following sources were identified:

1) a paper by Sutton and Roemmich (2001), detailing the long term climatology of the ocean temperatures off north-eastern New Zealand;
2) the Global Temperature-Salinity Profile Program (GTSPP) database (OOG: GTSPP, 2006), two profiles within 100 km of the model grid from September 2003; and
3) the World Ocean Database 2005 (WOD) (Boyer *et al.*, 2006), numerous (> 15) profiles within the model grid between 1978 – 2003.

Initial temperatures (during September 2003) were specified in the oceanic regions of the model domain based on two eXpendable-Bathy-Thermograph (XBT) records from the GTSPP database (OOG: GTSPP, 2006). Two profiles were available within 100 km of the model's northern boundary on 8 and 13 September 2003 (18 and 13 days prior to the model start). Surface layer (0-5 m depths) temperatures were inferred from AVHRR SST data co-incident with the model start time.

Neither the GTSPP of the WOD databases contained salinity profiles near the offshore regions of the model domain within several months of the model start time. Subsequently, historic offshore salinity profiles from the months of August, September, and October between 1978 and 2001 were assessed from both the GTSPP and WOD datasets. 'Seasonally typical' salinity profiles were identified and applied to the model for the initial offshore salinity profiles.

5.6.1.6.2 A NOVEL APPROACH TO THE OFFSHORE BOUNDARY CONDITION PROBLEM

The designation of offshore boundary conditions (temperature and salinity) represents a unique challenge in continental shelf modelling efforts. The offshore boundary by definition will be a significant distance from shore and often out of reach for sampling and profiling without a substantial ocean going vessel. In the absence of frequently measured time-series of profiles, supplementary methods must be employed.

Temperature profiles within 100 km of the model domain were extracted from the GTSPP and WOD datasets (Figure 5.10). Themocline locations were assessed from the 79 profiles (1978-2001) based on a sharp change in the temperature-depth gradient (Figures 5.10 and 5.11). Thermocline depths, when plotted as a function of time (Figure 5.11) indicate a gradual onset and deepening from October, along with a relatively rapid breakdown during winter, consistent with observations made by Sutton and Roemmich (2001).

In those profiles where a thermocline was observed, the temperature gradient in the upper layer had a mean value of -0.022 $^{o}Cm^{-1}$. The profiles (Figure 5.10) indicate that below 200 m the seasonal signal is weak, again consistent with Sutton and Roemmich (2001), and for the purposes of the model boundary condition are considered to remain constant through time.

To specify temperatures for the model layers a MATLAB® based model was developed to create a temporally and spatially varying open ocean temperature profile boundary condition based on:

1) time-interpolated 3-day remotely sensed SST at each grid point along the boundary;
2) a linear temperature profile from the surface through to the depth of the thermocline, with both the temperature gradient (-0.022 $^{o}Cm^{-1}$) and thermocline depth being based on 79 temperature profiles between 1978 and 2003 in the immediate area (Figures 5.10 and 5.11);
3) an exponential decay profile between the characteristic thermocline depth and temperature and a theoretical non time-varying temperature at 200 m depth of 14.5^{o}C (consistent with observations ±2^{o}C, Figure 5.10); and
4) temperatures in layers below 200 m depth are set to non time-varying values based on observed profiles in the immediate area (Figure 5.10).

This innovative solution to the open shelf boundary condition problem creates characteristic and reliable temperature profiles based on both time-series of SSTs and historically observed profiles in the immediate vicinity.

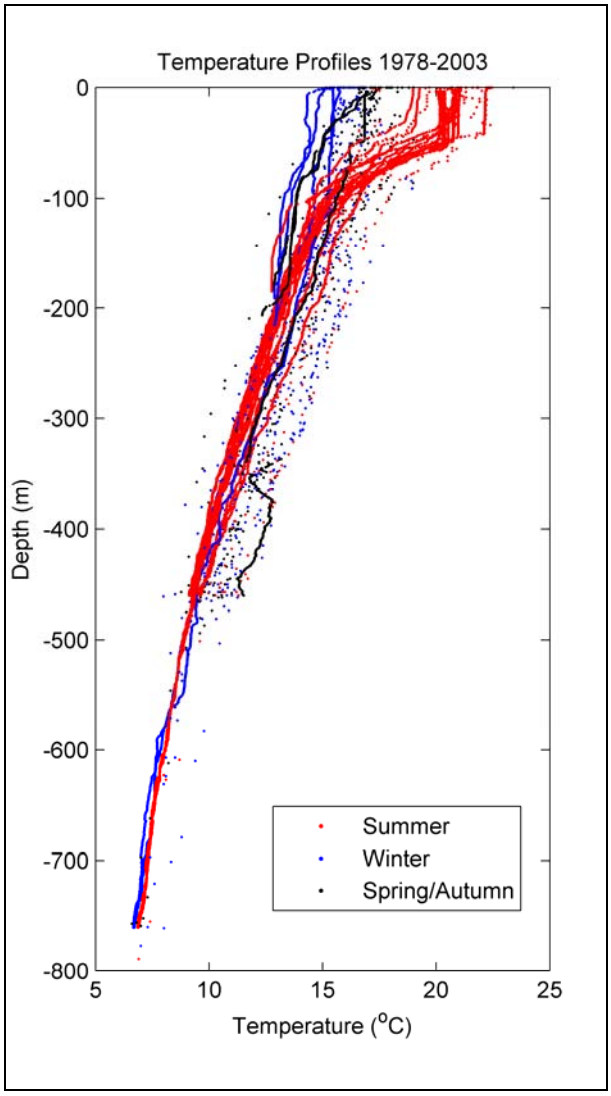

Figure 5.10 Temperature profiles within 100 km of the open boundaries between 1978 and 2003 from the GTSPP, WOD'05 and CTD surveys (n = 79). Temperatures during summer plotted as red dots, winter as blue dots and spring/autumn as black dots. Note the strong thermocline developed during summer between ~40 and 100 m water depth.

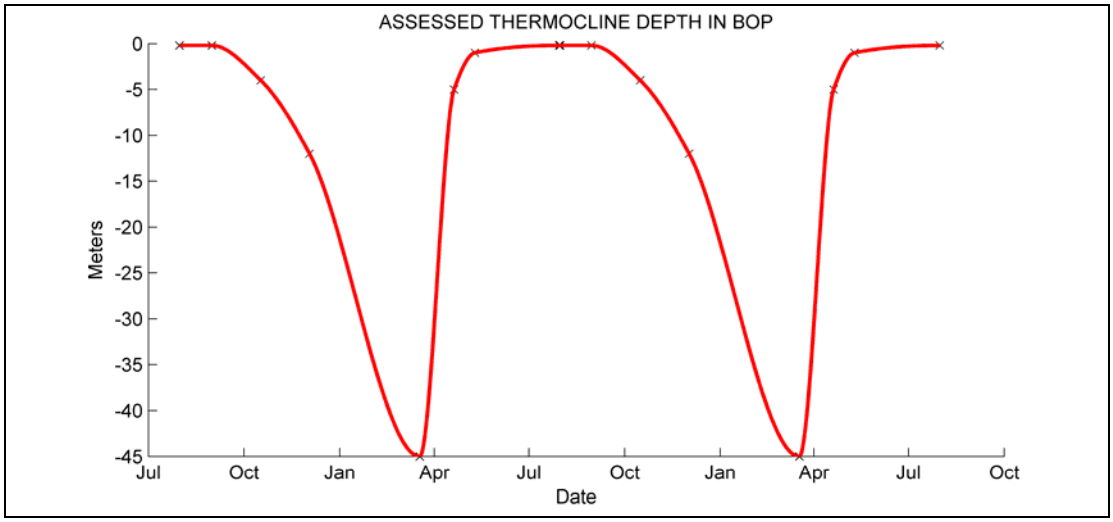

Figure 5.11 Seasonal variability in thermocline depth as assessed from 79 temperature profiles near the open boundaries. Note the slow development and deepening of the thermocline and the relatively rapid breakdown of stratification, consistent with observations by Sutton and Roemmich (2001).

Open boundary conditions specifying salinity profiles do not present similar problems. By their nature the open boundary conditions are predominantly in offshore waters where salinity variability due to freshwater is limited. There are no major (or minor) river systems near the intersection of the open boundaries and the shallower nearshore waters (Figure 5.9). A temporally and spatially constant salinity boundary condition was applied, consistent with data from the GTSPP and WOD'05.

5.6.2 MODEL CALIBRATION AND MODEL-DATA COMPARISONS

The model calibration interval covers 69 days (26 September 2003 to 4 December 2003). This period, commencing at a time of weak thermal stratification (Figure 5.11), provides some degree of flexibility in the hot-start temperature profiles. Though the hot-start file was inferred from the best available data, there are limitations, and starting the model at a time of weak thermal stratification is a strategy to minimise these.

The calibration period also presents a challenge for the model to replicate the onset and development of the stratification of the model, providing a suitable test of the model's ability to resolve observed temperature changes though the water column.

Data obtained during the calibration period includes long-term records of velocities and temperatures at the Pukehina 65 m site (Figure 5.8), a long-term record sea levels at Moturiki Island, and two CTD surveys (17 October 2003 and 3 December 2003) covering the Pukehina, Whakatane and Opotiki transects (Figure 5.8), providing both a spatially and temporally comprehensive dataset on which to test the model's performance.

5.6.2.1 CALIBRATION PARAMETERS: TURBULENCE, VISCOSITY AND DIFFUSIVITY

Turbulence in the ocean leads to dissipation and mixing over a range of scales. Eddy viscosity and diffusion formulations and coefficients (both horizontal and vertical) parameterise this process within the model. Eddy viscosities represent the turbulent transfer of momentum, while eddy diffusivities represent the turbulent diffusion of conservative properties (*e.g.* heat, salt).

The nature and scale of turbulence is a property of the flow field itself rather than an inherent property. The vertically stratified nature of most seas requires that any vertical displacement overcome this buoyancy force. As a result, horizontal turbulence and mixing is much more prevalent than that occurring in the vertical plane. This is generally represented through much larger coefficients in the horizontal plane cf. the vertical. While there are established ranges for each of these properties when modelling the marine system, there is some degree of flexibility, allowing a calibration for the best fit with observed data.

5.6.2.1.1 HORIZONTAL EDDY VISCOSITIES

Horizontal eddy viscosities within the 3DD model are typically set between 0.1 – 5 m^2s^{-1}, with the larger values often applied to coarser grids (Black, 1995). Large scale ocean circulation models can have values in excess of 1000 m^2s^{-1} (Cox, 1970; Cox, 1975), reflecting the requirement to have all turbulence smaller than regional scale eddies dissipated i.e. it sets the minimum boundary to which horizontal variance is oserved.

Due to the unique characteristics of the Bay of Plenty model domain (both nearshore and far-offshore flow fields) a spatially variable horizontal eddy viscosity coefficient was implemented. This arises from the need to resolve flow field eddies of scales ~10-15 km near the coast, whilst also providing enough dampening to prevent spurious results in deeper offshore regions. The coefficient is based on the local bathymetry and varies smoothly from 0.1 m^2s^{-1} near the coast to 200 m^2s^{-1} in water deeper than 100 m (Table 5.3).

5.6.2.1.2 VERTICAL EDDY VISCOSITIES

Vertical eddy viscosities are modelled based on mixing length and Richardson number formulations (Section 5.4), utilising the modelled flow and stratification characteristics to best represent momentum transfer. The calibrated coefficient of 10^{-4} m^2s^{-1} (Table 5.3) is reasonably consistent with other published values from similar environments (*e.g.* Hasami and Suginohara, 1999, Davies and Xing, 2003).

5.6.2.1.3 HORIZONTAL EDDY DIFFUSIVITIES

Typical measured horizontal diffusivities range from 8 x 10^2 m^2s^{-1} (geostrophic scales, *e.g.* Holloway, 1986; Ledwell *et al.*, 1998; Benetiz-Nelson *et al.*, 2000) to 1-3 m^2s-^{1} (open coastal environments, Ledwell *et al.*, 1998).

The calibrated value (10 m^2s^{-1}, Table 5.3) represents a balance within the modelled environment, including aspects of both local and regional (geostrophic) scales.

5.6.2.1.4 VERTICAL EDDY DIFFUSIVITIES

Calibration of vertical diffusivities through the application of a modelled parabolic Richardson number, based on modelled stratification (Section 5.4) proved troublesome. Adjustments to the model code allowing the use of a fixed Richardson number aided the model's replication of vertical salinity and temperature profiles. The effect of a fixed diffusion coefficient is to produce a smoother diffusion gradient through the water column.

While the use of a fixed Richardson number is a simplification from the more standard parabolic formulation, it is not without precedent. Davies and Xing (2003), who

tested the effects of a fixed coefficient of 2 x 10^{-4} m^2s^{-1} against a varying value, failed to note any significant negative impacts.

Calibration tests indicated the best-fit value for vertical eddy diffusivity to be 10^{-4} m^2s^{-1}. Encouragingly, this result fits well with actual measured values (often determined by tracer dilution) of vertical eddy diffusivities in similar shelf type environments, which are consistently in the range of 10^{-5} – 10^{-3} m^2s^{-1} (Silker, 1972; Young and Silker, 1974; Largier, 1994; Kunze and Toole, 1997; Ledwell *et al.*, 1998; Hasumi and Suginohara, 1999).

Table 5.3 Numerical parameters for wind-driven three-dimensional baroclinic modelling of the Bay of Plenty using the model 3DD.

Parameter	Value
Time step	10 seconds
Roughness length	0.002 m
Horizontal eddy viscosity coef.	0.1 to 200 m^2s^{-1} (nearshore – offshore)
Vertical eddy viscosity coef.	10^{-4} m^2s^{-1}
Horizontal eddy diffusivity coef.	10 m^2s^{-1}
Vertical eddy diffusivity coef.	10^{-4} m^2s^{-1}
Model time start (t_0)	26/9/2003 0:00 NZST
Grid resolution	3000 m x 3000 m
Grid dimensions	69 x 38
Grid orientation	0^o true
Grid origin	276100 mE, 633900 mN, NZMG1949
Grid latitude (centre)	-37^o
Coastal slip	95 %
Effective depth	0.03 m
Drying height	0.05 m
North boundary	Specified temperatures and salinities, geostrophic-Coriolis satisfying sea levels.
East boundary	Specified temperatures and salinities.

5.6.2.2 RESOLVING TIDAL AND INVERSE BAROMETRIC INFLUENCES ON SEA LEVELS

To compare model output to observed sea level records, the observed data must first be checked for outliers, filtered to remove tides and corrected for additional influences not incorporated into the model (such as the sea level response to atmospheric pressure).

A long term record of Moturiki Island (Figure 5.8) sea level elevations were de-tided by removing the harmonic tidal signal (T_TIDE, Pawlowicz *et al.*, 2002) and low pass filtering (36 hour recursive butterworth). The original tidal signal explained 97.8% of the variance in the raw sea level oscillations at Moturiki Island.

In addition to the tidal signal, barometric pressure is a low-frequency forcing function on sea levels and its direct influence is not incorporated into the model. It is common practice to correct sea levels for the inverted barometer (IB) effect prior to comparison with model output or subsequent data analysis. Traditional corrections for the IB

effect on sea levels involve an adjustment of 10 mm in the sea level for a unit change in atmospheric pressure (hPa):

$$\Delta\zeta = -10\Delta P_{atm} \qquad \textbf{Equation 5.23}$$

where $\Delta\zeta$ is the change in sea level (mm) and ΔP_{atm} is the change in atmospheric pressure (hPa) (*e.g.* Pond and Pickard, 1983; Huyer, 1984; Goring, 1995; Bell and Goring, 1996).

A linear regression of de-tided sea-levels at Moturiki (2 year record) with local barometric pressure (Tauranga Airport, <2 km separation) indicated a best fit relationship of:

$$\Delta\zeta = -6.6\Delta P_{atm} \qquad \textbf{Equation 5.24}$$

with the IB effect accounting for 59% of the variance (R^2 = 0.59, significant at the 95% level) in the de-tided sea-levels. This represents a weaker IB effect (6.6 *cf.* 10) than the 'traditionally' applied relationship. Goring (1995) notes, however, that sites along New Zealand's eastern shorelines generally respond to changes in barometric pressure at lower than 'traditional' levels. The present result is consistent with this conclusion. Sites along New Zealand's western shores were found to respond to greater degrees, a general result exposure to the predominant westerly wind events (Goring, 1995).

5.6.2.3 MODEL-DATA COMPARISONS: SEA LEVELS

The calibrated model replicates the general patterns of de-tided (and IB corrected) sea levels at Moturiki Island (Figure 5.12a). However, several shorter term (< 3-4 day periods) events are either not replicated or replicated with smaller magnitudes than those observed.

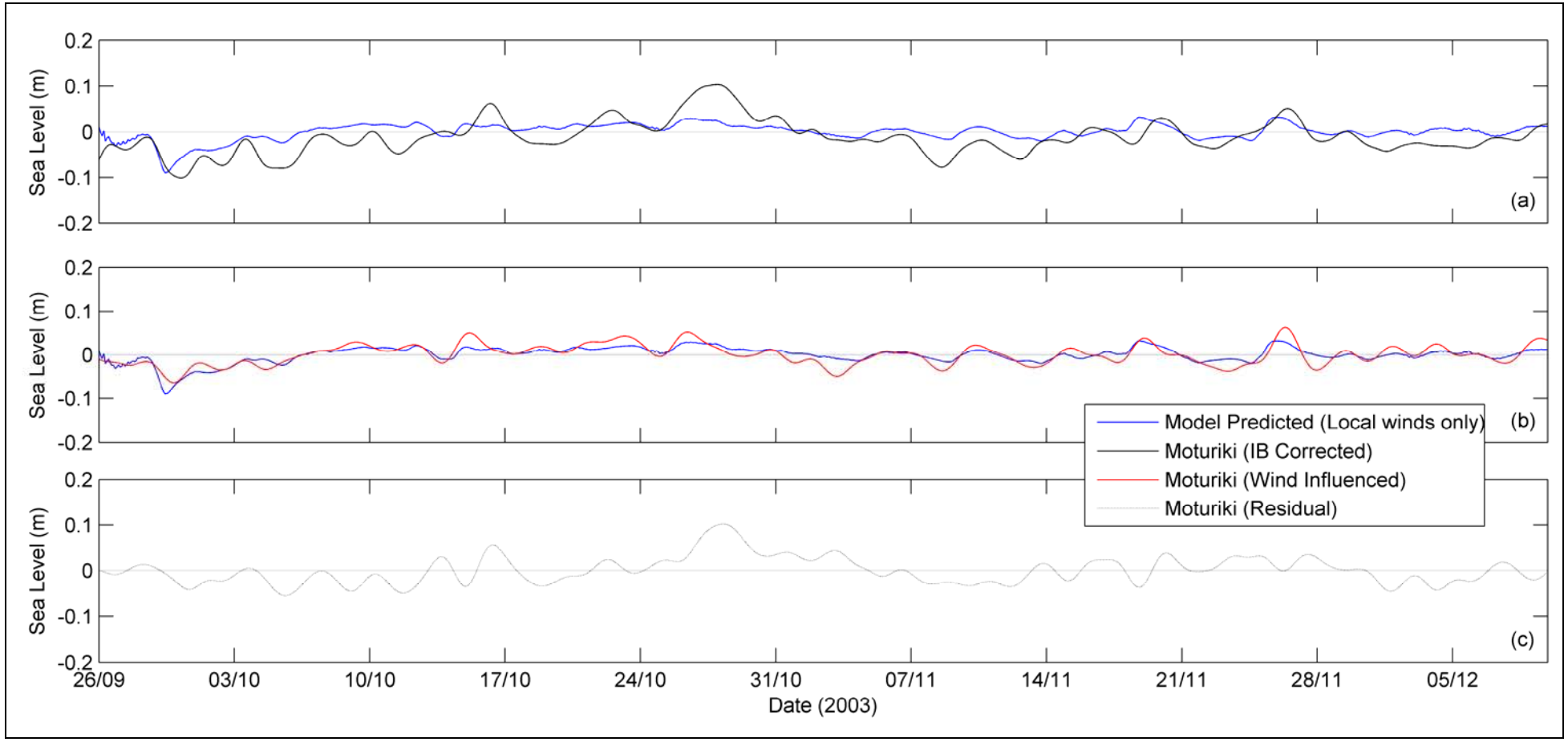

Figure 5.12 Observed and model predicted sea levels at Moturiki Island. The model predictions follow the general trends of the IB corrected sea levels (a), however several peaks are not replicated. Wind influenced sea levels at Moturiki are well replicated by the wind driven model (b) with the correlation between observed (wind influenced) and model predictions achieving an R value of 0.82. Residual observed sea levels at Moturiki (c) cannot be explained by local winds and alternate forcing mechanisms must be investigated.

Considering that the model under question is forced solely by local wind fields, it is logical to compare the model output to those sea level variations which can be explained by the local winds. To investigate this further, multiple lagged correlations were carried out between along and cross-shelf wind velocities and the de-tided IB corrected sea levels between January 2003 and December 2004 (Table 5.4).

Table 5.4 Multiple linear regression coefficients of wind velocity components and de-tided IB corrected sea levels at Moturiki Island. The correlation coefficient is significant at the 95% level.

Regression coeff (along-shelf wind velocity) (mm/ms^{-1})	Regression coeff (cross-shelf wind velocity) (mm/ms^{-1})	Correlation coefficient	Lag interval (S.L following wind) (hrs)	Duration of data (days)
-10.5 ± 0.3	-0.6 ± 0.2	0.58	13	718

Peak correlations were identified with a lag interval of 13 hours (sea levels following winds). Along-shelf winds from the NW are followed (13 hrs) by a depression in coastal sea level at a rate of 10.5 mm/ms^{-1} (Table 5.4). This pattern is dynamically consistent with the upwelling dynamics previously identified within the Bay of Plenty (Chapter 4). It has been observed (Chapter 4) that upwelling favourable along-shelf winds from the NW generate circulation dynamics which leads to an along-shelf (SE) geostrophic flow. This geostrophic flow must be in dynamic balance with a cross-shelf sea level gradient, reflected by depressed coastal sea levels during upwelling episodes.

This observed relationship between winds and sea levels at Moturiki initially seems inconsistent with similar analyses performed by Goring (1995) who failed to find any significant relationships between the same parameters at Moturiki Island between 1984 and 1991. Goring (1995), however, performed his analyses with co-incident winds and sea levels (no lag interval) as opposed to an initial lagged cross-correlation, as carried out here, to determine the peak lag interval for the relationship. In addition, there is physical justification and evidence for the phenomena as a result of the geostrophic balance set up by the upwelling circulation observed from the Pukehina ADP deployment (Chapter 4).

The local wind driven model effectively replicates (R=0.82) wind influenced sea levels at Moturiki Island (Figure 5.12b). However, excess variability in residual sea levels (non wind influenced portion, Figure 5.12c) remains unaccounted for by the local wind driven model. This unexplained variability is likely to be associated with variability in local water velocities. Given the inability to replicate excess sea level variability, it is likely that a similar proportion of the velocity fields will also remain unexplained. Bell and Goring (1996) observed frequent unexplained variations in residual sea levels which could not be explained by local winds or locally generated wave effects (Figure 5.12c in this analysis). They concluded that, at Moturiki, the variation in these residual sea levels is caused by either waves propagating into the area, potentially from tropical cyclones *etc* located many hundreds of kilometres to the north, or from coastal trapped waves travelling around East Cape. Attempts to

incorporate these (and other) external influences into the model are made in subsequent sections.

5.6.2.4 RESOLVING WIND INFLUENCED CURRENTS

In general, numerical modelling of open-coast shelf circulation and hydrodynamics is difficult (Huyer, 1990; Huthnance, 1995; Csanady, 1997; Davies and Hall, 2002) due to large spatial-scale events propagating into the modelled area, *e.g.* oceanic currents and coastal trapped waves. Such features are generated outside the model domain, and, unless incorporated into the model boundaries, remain unaccounted for. The present model represents solely the influence of local wind-driven and density-driven flows on the shelf.

We have seen from Chapter 4 the correlation between current vectors and wind stresses. Here, this observation is expanded to multiple linear regressions using both along and cross-shelf wind components (Table 5.5). Lagged multiple cross-correlation analyses identified regression coefficients and the lag intervals at which the correlation coefficients were maximised. Peak lag intervals occurred between 8 and 24 hours for along-shelf currents (winds preceding currents) and between 12 and 17 hours for cross-shelf currents, largely consistent with the previous analyses (Chapter 4). Using these regression coefficients (Table 5.5), an estimate of the local wind driven component of the ADP current velocities can be made (Figure 5.13). Model results (local wind and density driven currents) were compared to both the ADP data (tides removed and low pass filtered, 36 hour recursive butterworth), and also to the estimated wind influenced currents (calculated from low pass filtered wind velocities using coefficients from Table 5.5) as time-series (Figures 5.13 and 5.14), scatter plots (Figures 5.15 and 5.16), and as progressive vectors (Figure 5.17).

Table 5.5 Multiple linear regression coefficients and peak lag intervals of wind stress components and low-passed water velocities from the ADP. ADP velocities depth averaged over model layers. Data duration is 70.8 days (September-December 2003). All correlation coefficients significant at the 95% level.

	Depth range (model layer)	Regression coeff (along-shelf wind stress) (ms^{-1}/Pa)	Regression coeff (cross-shelf wind stress) (ms^{-1}/Pa)	Correlation coefficient	Lag interval (currents following wind) (hrs)	Duration of data (days)
Along-shelf currents	5-15 m (2)	2.41 ± 0.17	-1.02 ± 0.17	0.57	13	70.8
	15-35 m (3&4)	2.65 ± 0.15	-0.70 ± 0.16	0.65	15	70.8
	35-50 m (5)	3.22 ± 0.16	-0.82 ± 0.16	0.70	16	70.8
	50-70 m (6)	2.78 ± 0.15	-0.81 ± 0.15	0.67	19	70.8
Cross-shelf currents	5-15 m (2)	0.24 ± 0.06	-0.60 ± 0.06	0.43	11	70.8
	15-35 m (3&4)	-0.52 ± 0.06	-0.17 ± 0.06	0.49	8	70.8
	35-50 m (5)	-1.31 ± 0.06	0.39 ± 0.06	0.75	9	70.8
	50-70 m (6)	-1.60 ± 0.07	0.48 ± 0.08	0.72	10	70.8

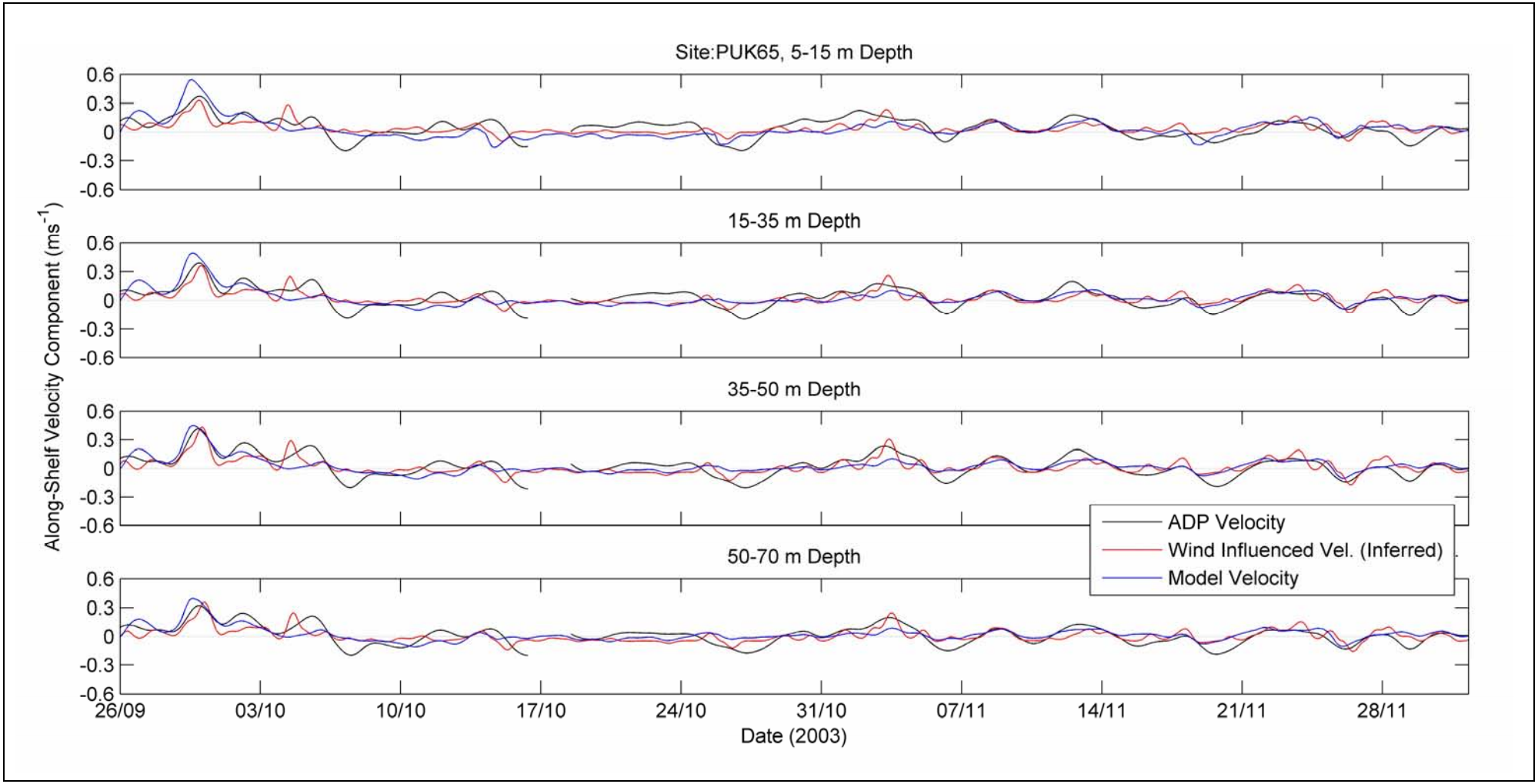

Figure 5.13 Measured and modelled (wind and density-driven) along-shelf velocities throughout the water column at the Pukehina 65 m site. Measured data low-pass filtered with a recursive butterworth filter (36 hr cut-off) to remove tidal and other short term oscillations not incorporated into the model. ADP serviced between 17 and 18 October 2003.

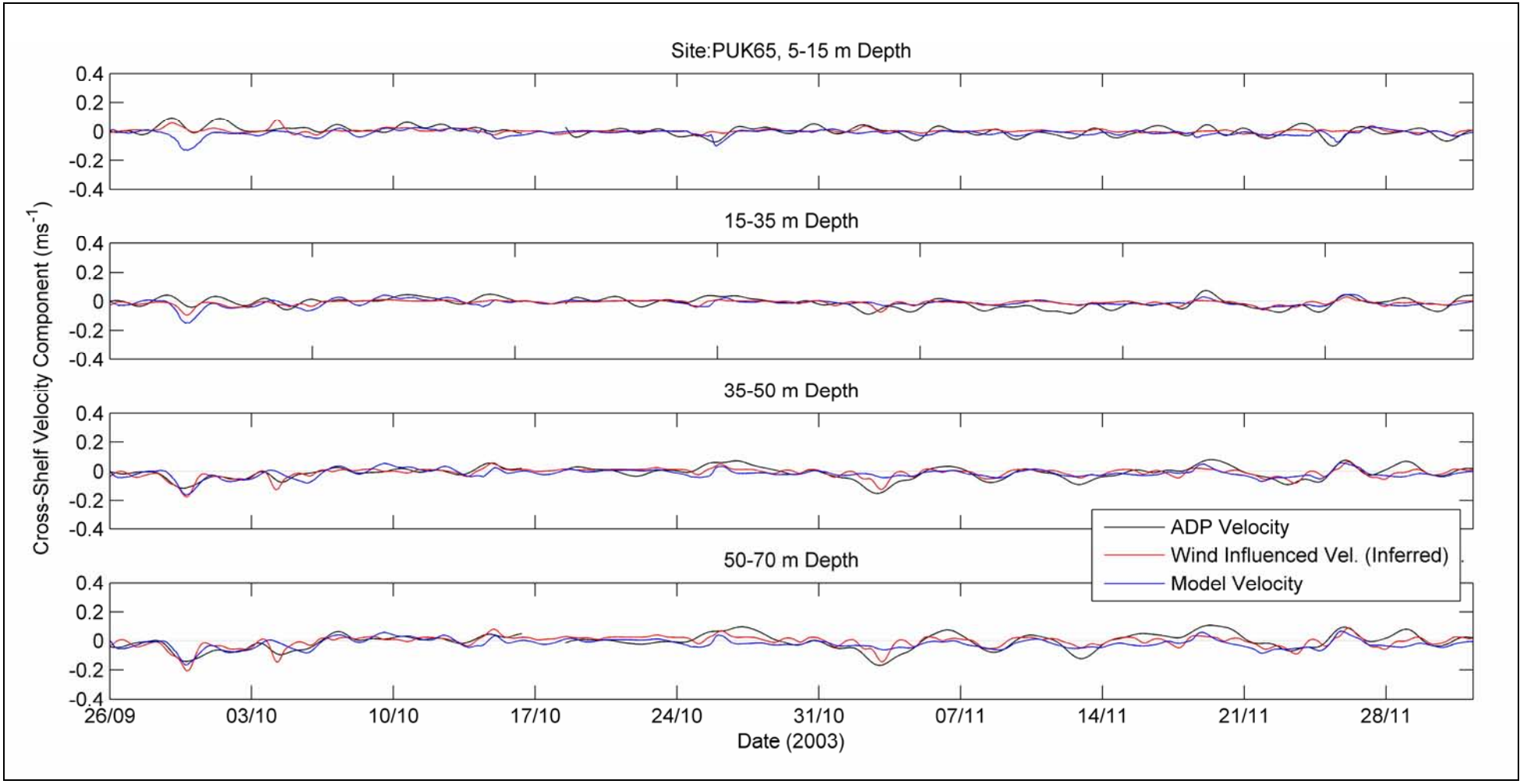

Figure 5.14 Measured and modelled (wind and density-driven) cross-shelf velocities throughout the water column at the Pukehina 65 m site. Measured data low-pass filtered with a recursive butterworth filter (36 hr cut-off) to remove tidal and other short term oscillations not incorporated into the model. ADP serviced between 17 and 18 October 2003.

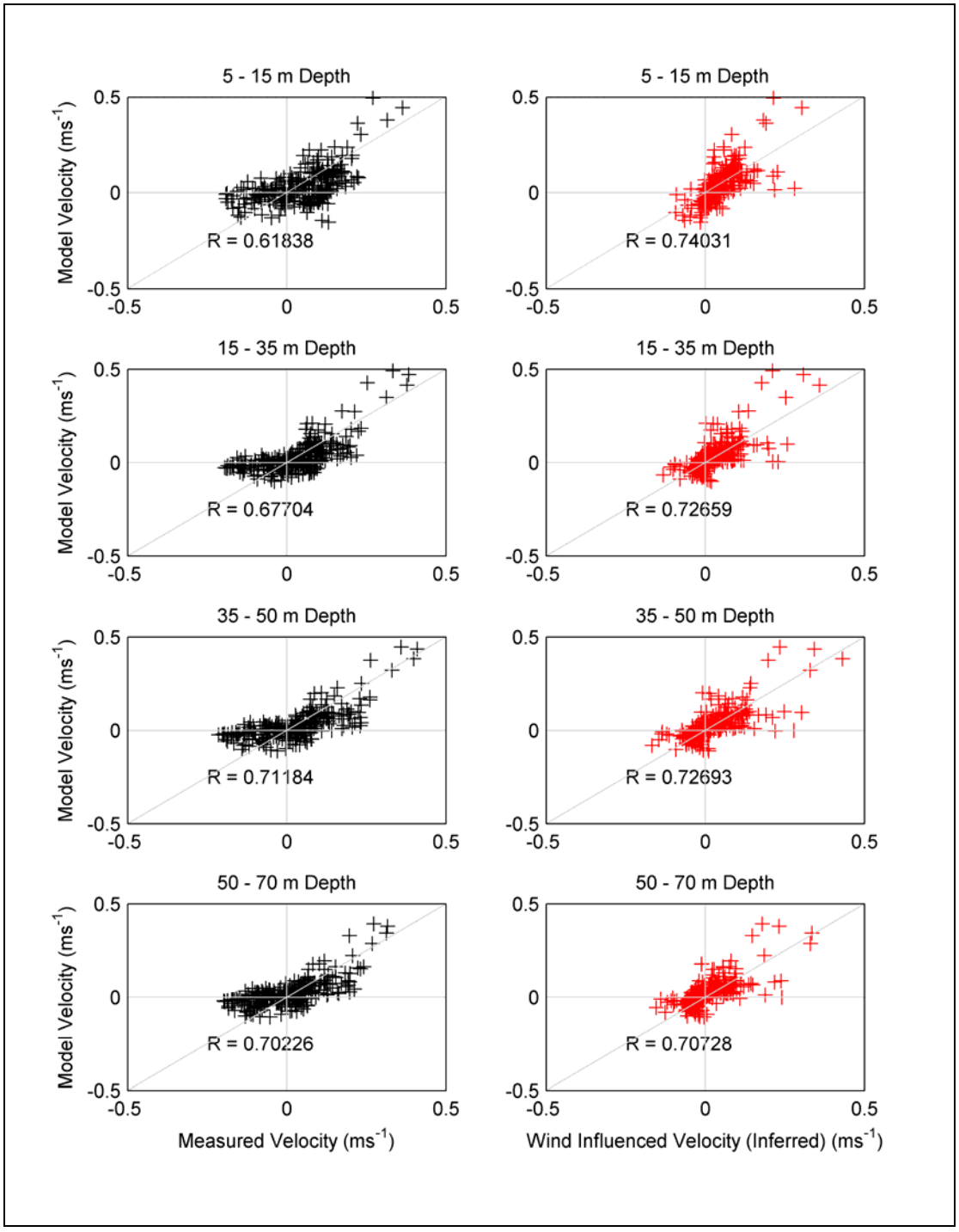

Figure 5.15 Scatter plots and correlation coefficients of measured (ADP), inferred (local wind influenced component) and modelled along-shelf velocities at the Pukehina 65 m site. Time series data were decimated at 6 hourly intervals. All correlation coefficients significant at the 95% level.

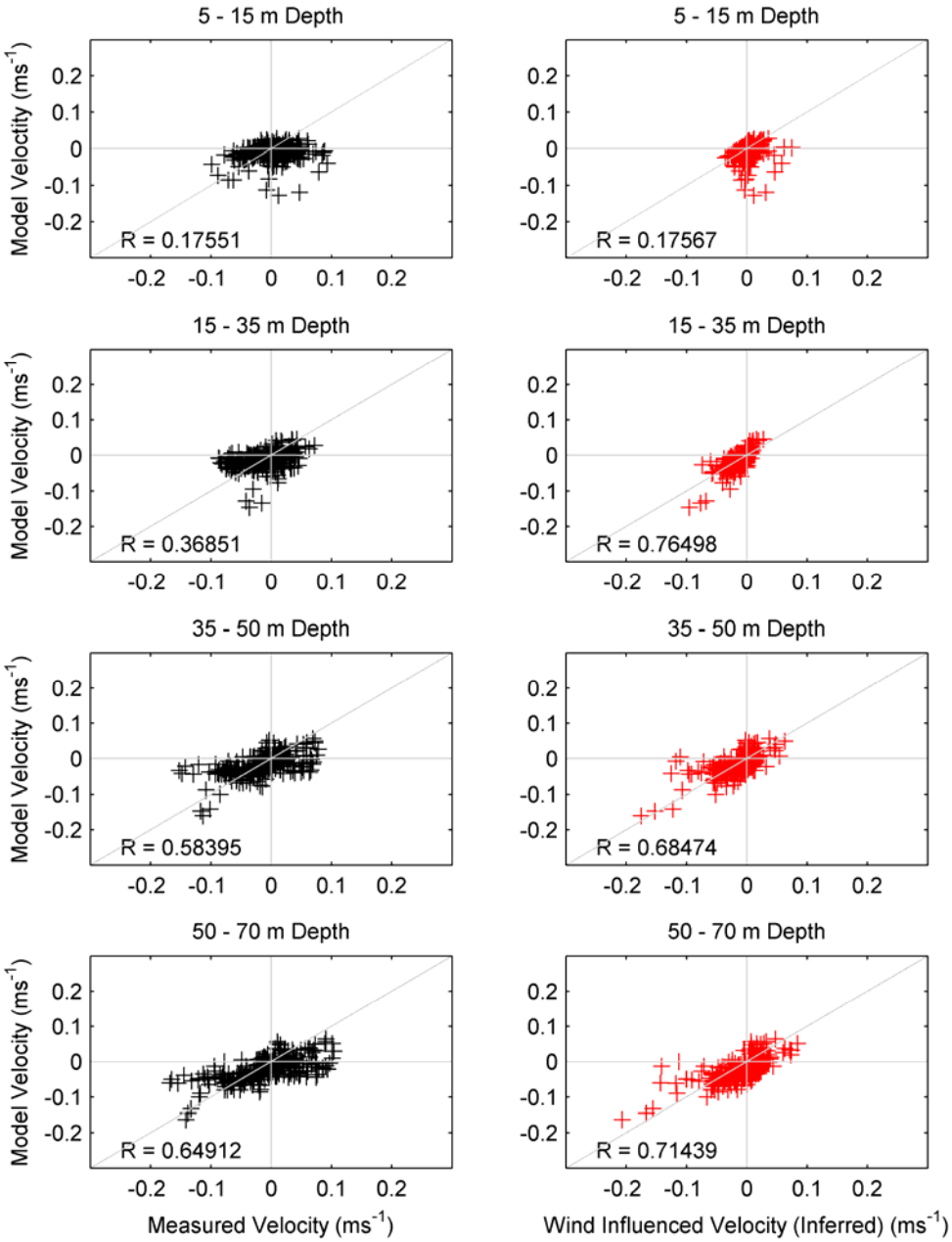

Figure 5.16 Scatter plots and correlation coefficients of measured (ADP), inferred (local wind influenced component) and modelled cross-shelf velocities at the Pukehina 65 m site. Time series data were decimated at 6 hourly intervals. All correlation coefficients significant at the 95% level.

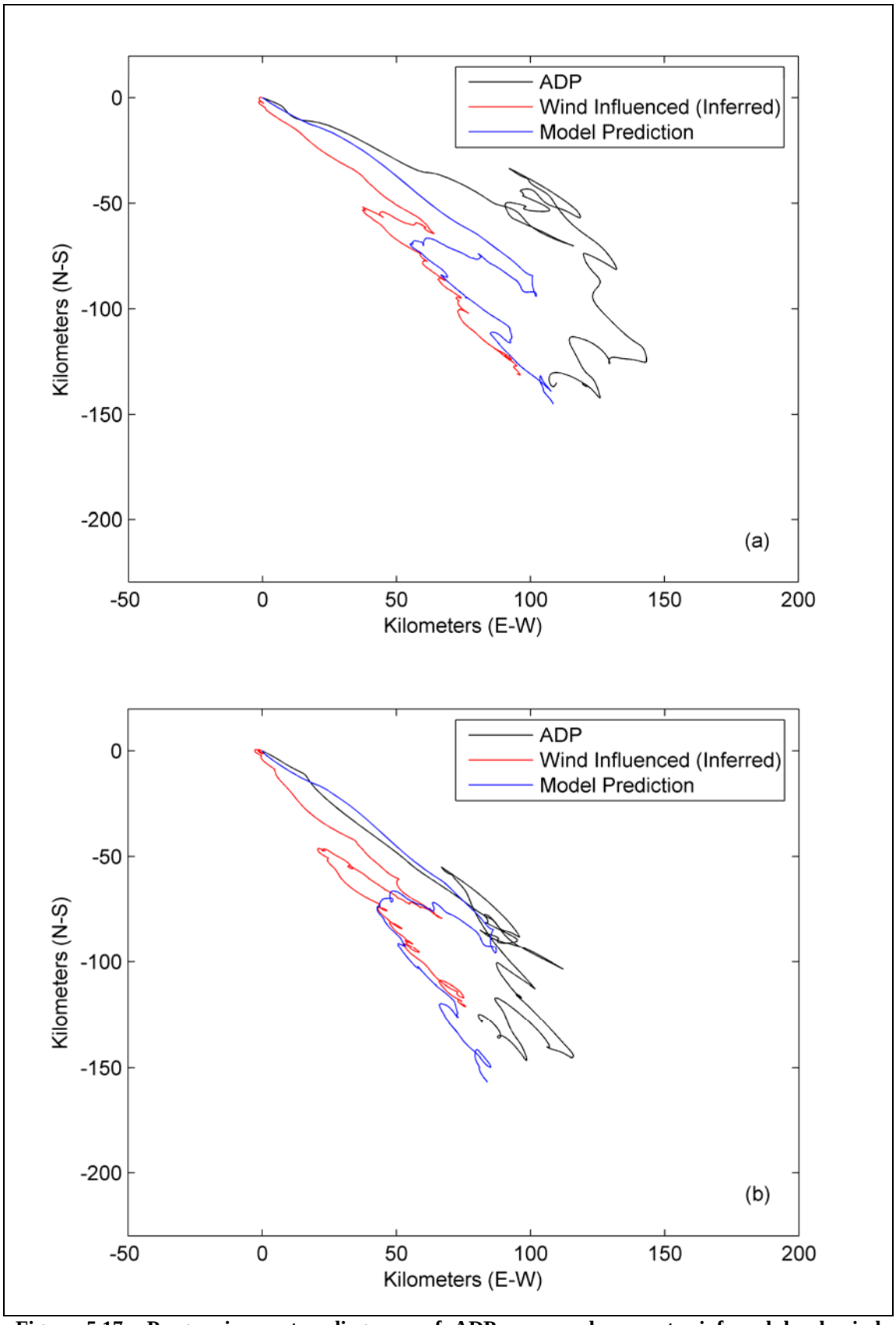

Figure 5.17 Progressive vector diagrams of ADP measured currents, inferred local wind influenced currents, and model predicted currents at the Pukehina 65 m site (15 – 35 m (a) and 35 – 50 m (b)) between 26 September 2003 and 2 December 2003 (67 days). Vectors originate at (0,0) and represent the theoretical passage of particles in time past the site, they do not represent lagrangian paths. No vectors have been plotted during the time the ADP was serviced, and those before and after the servicing have been plotted 'nose on tail'.

5.6.2.5 MODEL-DATA COMPARISONS: CURRENTS

The calibrated model effectively reproduces the general trends in the ADP current meter record, though fails to replicate some of the shorter term (< 5 day periods) variability in both cross-shelf and along-shelf directions (Figure 5.13 and 5.14). Inferred local wind influenced currents indicate the observed ADP currents contain some external influences (not local winds) at times when the model fails to replicate observed short term variability. Examples occur on 7/10/2003, 27/10/2003, and 6/11/2003 (Figure 5.13), where the ADP indicates relatively strong flows to the NW (-ve along-shelf) which are not associated with the local winds or represented in the local wind and density driven model output. These flows remain unexplained by the model as it stands and require further investigation to determine their forcing mechanisms and influences.

The model accurately predicts the general magnitudes of observed (ADP) along-shelf and cross-shelf velocities throughout the water column in addition to the relative magnitudes of each component (Figure 5.13 and 5.14). The model is more accurate at replicating along-shelf than cross-shelf ADP flows (Figures 5.15 and 5.16), however, when compared to inferred wind influenced current components the model replicates both along and cross-shelf currents equally well.

Progressive vector diagrams (Figure 5.17) can indicate any residual 'drift' of numerical models in addition to highlighting a model's ability (or inability) to replicate specific directions of observed currents (Emery and Thomson, 2004). The progressive vectors indicate that the general replication of the ADP signal is satisfactory, with the net modelled movement over the 67 days being remarkably similar to that of the ADP. However, consistent with the time-series results, the model fails to replicate some observed short-term variability in the ADP records. The progressive vectors indicate that this short-term variability is inconsistent in direction (Figure 5.17). If the variability were consistent in direction, a noticeable drift would be apparent from these progressive vectors.

The model replicates local wind inferred progressive vectors better than raw ADP records (perhaps more than the differences in regression coefficients suggest, Figures 5.15, 5.16, and 5.17).

It can be concluded, that the model (driven by local winds and density) adequately replicates the general features of the observed currents, and replicates effectively the component of those flows which are driven by local winds (inferred from multiple lagged correlations). It is anticipated that further work investigating additional forcing mechanisms (*e.g.* large scale oceanic boundary currents, coastal trapped waves [CTWs]), and their incorporation into the model's boundary conditions will enhance the model's ability to replicate the observed residual currents.

5.6.2.6 SST AND A DATA ASSIMILATION SCHEME

An issue encountered during calibration runs was the gradual, though consistent, cooling of the model's surface layers throughout the model run. Given the uncertainty of the meteorological data (over the large spatial scales being modelled) such trends cannot be cured through simple adjustment of model coefficients, as the multiple terms in the heat balance equations interact in a complex fashion. For example, the wind induces substantial heat losses, and thus is critical to the success of heat flux modelling. However, adjustments to the wind for the purposes of the heat balance will have a negative effect on wind driven current predictions.

Ocean/atmosphere heat fluxes involve a subtle balance between several large terms (solar inputs and various heat loss terms). These terms rely on measured variables which can vary spatially and are not precisely known throughout the model domain (*e.g.* incoming solar radiation, air temperatures, humidity etc). Small imbalances between the calculated terms can, over long periods of time, lead to modelled surface temperatures diverging from observed values.

To overcome this difficulty, a novel data assimilation scheme involving remotely sensed SSTs is applied. Data assimilation techniques have been relatively widely applied in meteorological and global ocean models (*e.g.* Derber and Rosati, 1989; Ghil and Malanotte-Rizzoli, 1991), though the assimilation of SSTs in coastal ocean models has been less common (Turner *et al.*, 2005; Andreu-Burillo *et al.*, 2007).

SSTs inferred from the AVHRR sensor (see Chapter 4 for details and validation) were used in a 'nudging' approach to steer the upper two model layer temperatures toward the inferred data with a 3-day frequency (3-daily SST retrievals). The 1-km resolution SST data were spatially smoothed (3x3 cells) resulting in a data with 3-km resolution, corresponding to the hydrodynamic model grid. Each 3 days temperatures in the surface layer (0-5 m) were updated with the spatially smoothed SST values, while those in the second layer (5-15 m) were scaled down by the observed upper water column temperature gradient of -0.022 $^{o}Cm^{-1}$ (Figure 5.10). Deeper layers did not suffer the same heat loss problem (as heat is only lost from the ocean surface), and thus remained at modelled values without any 'nudging' applied.

Such data assimilation techniques are at the forefront of coastal ocean modelling and lead to enhanced and more accurate short-term model predictions (Turner *et al.*, 2005). Accurate prediction of water temperatures is vital to ecological modelling (Chapter 7) due to its fundamental role in determining ecological process rates. The assimilation scheme developed for this project has subsequently been applied to another large coastal embayment with equally encouraging results (Harrison *et al.*, 2007)

5.6.2.7 MODEL-DATA COMPARISONS: TEMPERATURES

Time-series of water temperatures at the Pukehina 65 m site indicate that the model effectively reproduces both short and longer-term variability in observed temperatures (Figure 5.18). The magnitude and timing of diurnal temperature oscillation is reproduced well in the upper layer of the model. Short-term, diurnal variations in temperature are not captured as successfully in the deeper model layers at this site (Figure 5.18). This is likely caused by the light decay constants applied within the model being set to mean values obtained from a collective range of sites within the Bay of Plenty. While locally specific decay constants could improve the models ability at this site, this would be at the expense of other locations within the Bay of Plenty. This is highlighted by a comparison of observed and modelled temperatures at 18 separate sites, over 6 model layers and 2 separate time periods from CTD surveys (Figure 5.19). Thus, with the limitation of applying spatially uniform light decay constants, the model is replicating the time-series of temperatures effectively.

Notably, the third model layer (15-25 m) replicates the general trends of observed temperatures well (Figures 5.18 and 5.19). This layer does not benefit from the SST nudging scheme, and no artificially sharp gradients in temperature are being modelled as a result of the nudging of only the top two model layers.

Some small-scale variability between modelled and observed temperatures can be expected due to the physical dimensions of the grid. The modelled temperature represents the mean temperature over a 3000 x 3000 m x ‘layer depth’ box, while the measured temperature represents a single point and single depth (thermistor), a single point averaged over the layer depth range (CTD), or a 1000 x 1000 m cell of the ocean surface (AVHRR).

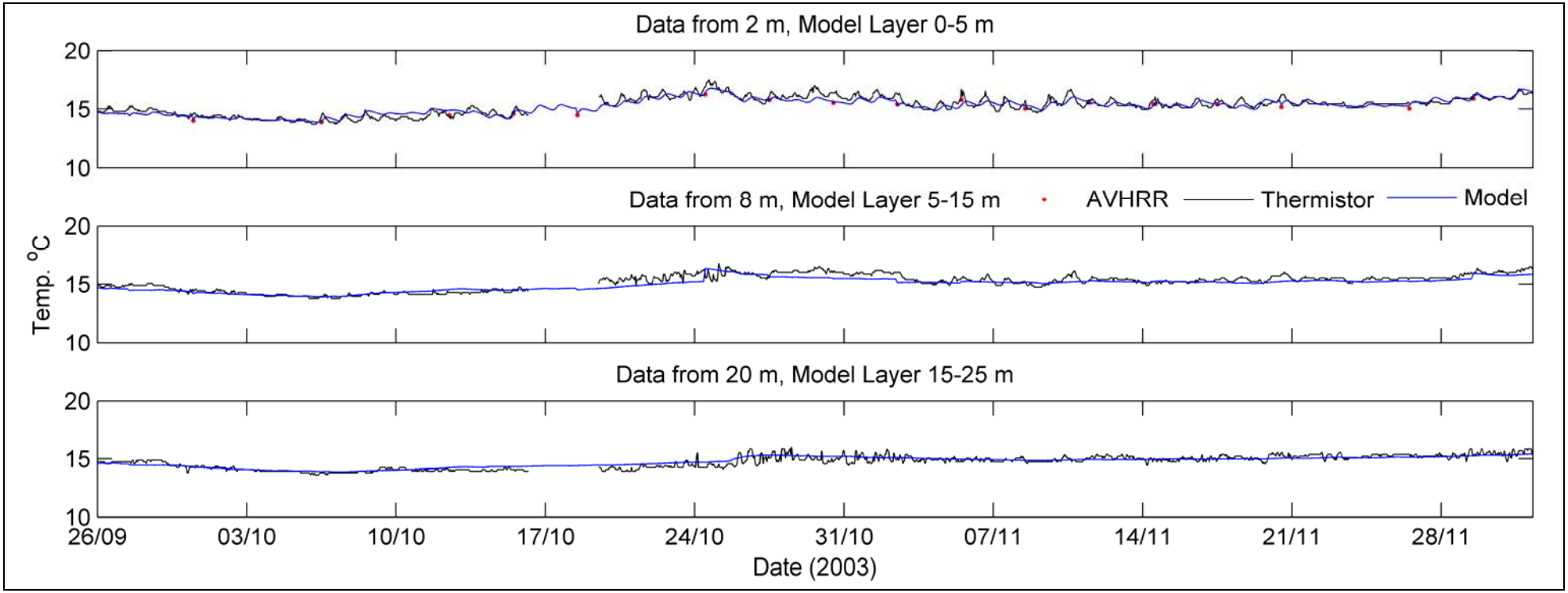

Figure 5.18 Time series of observed (AVHRR and thermistor) and modelled temperatures at the Pukehina 65 m site during the calibration period.

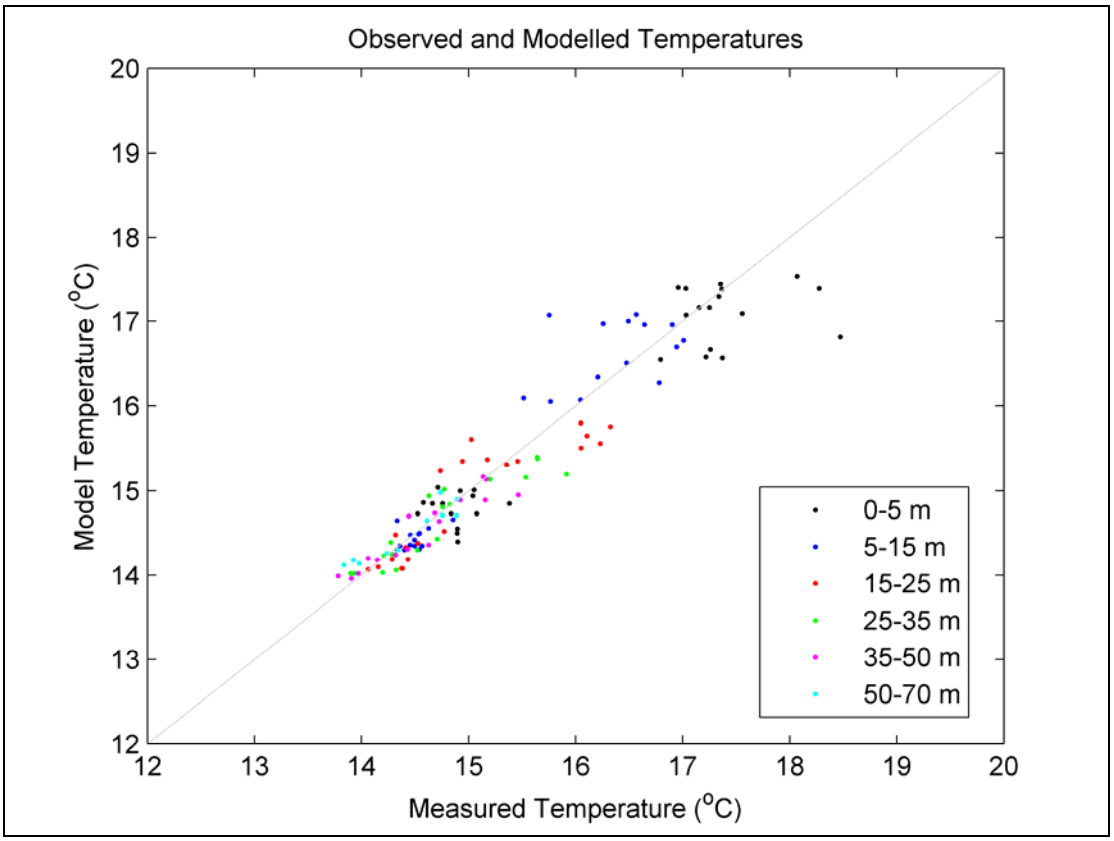

Figure 5.19 Measured and model predicted temperatures during the calibration period. Measured data from CTD casts at 18 individual sites (along 3 transects), and from two time periods (17/10/2003, and 3/12/2003). Depth of temperature measurement (averaged across model layers) indicated by colour of marker.

5.6.2.8 MODEL DATA COMPARISONS: SALT CONCENTRATIONS AND FRESHWATER INPUTS

Salt concentrations within the model were calibrated in conjunction with temperatures through the modification of the horizontal and vertical eddy diffusivity coefficients. Following a number of runs, best fit values were determined (Table 5.3). Comparisons to CTD data (17/10/2003 and 3/12/2003), indicated that modelled salinities reproduce observed values well in both a general (Figure 5.20), fluctuating (Figure 5.21), and spatial (Figure 5.22) sense.

Though the model predictions are relatively evenly spread either side of the 1:1 fit line (Figure 5.20), there is some degree of variance between observed and modelled salinities, especially in the upper model layers. Spatially variable salinity values could not be applied in the hot start file as no comprehensive dataset exists, requiring the model to gradually adjust to 'equilibrium' values over time from the uniform 35.3 ppt initial value. In addition, the comparison of a 3000 x 3000 m model cell with a point based measurement (CTD) may lead to some variance during evaluations.

Despite these restrictions, both modelled and observed salinities exhibit very similar variability (range) with depth in the water column (Figure 5.21). In addition to the

replication of general trends and variability in salinity, the general spatial pattern is reproduced (Figure 5.22).

The restrictions of the 'point based' CTD measurements are highlighted from salinity data shown in Figure 5.22. Along the central (Whakatane) transect, directly offshore from the Whakatane River mouth, the observed surface salinity was 34.3 ppt at the 10 m site, and 33.6 ppt farther offshore, at the 20 m site. There is insufficient data to determine the reliability or persistence of this unusual pattern of decreasing salinity offshore from a river mouth. This variance is, however, included in these data when comparisons are made to model predictions (*e.g.* Figure 5.20). If indeed the observed pattern is reliable and caused by some physical phenomena, its sub-grid size scale prevents the model from replicating these measurements (the two sites are separated by 1008 m, cf. grid resolution of 3000 m).

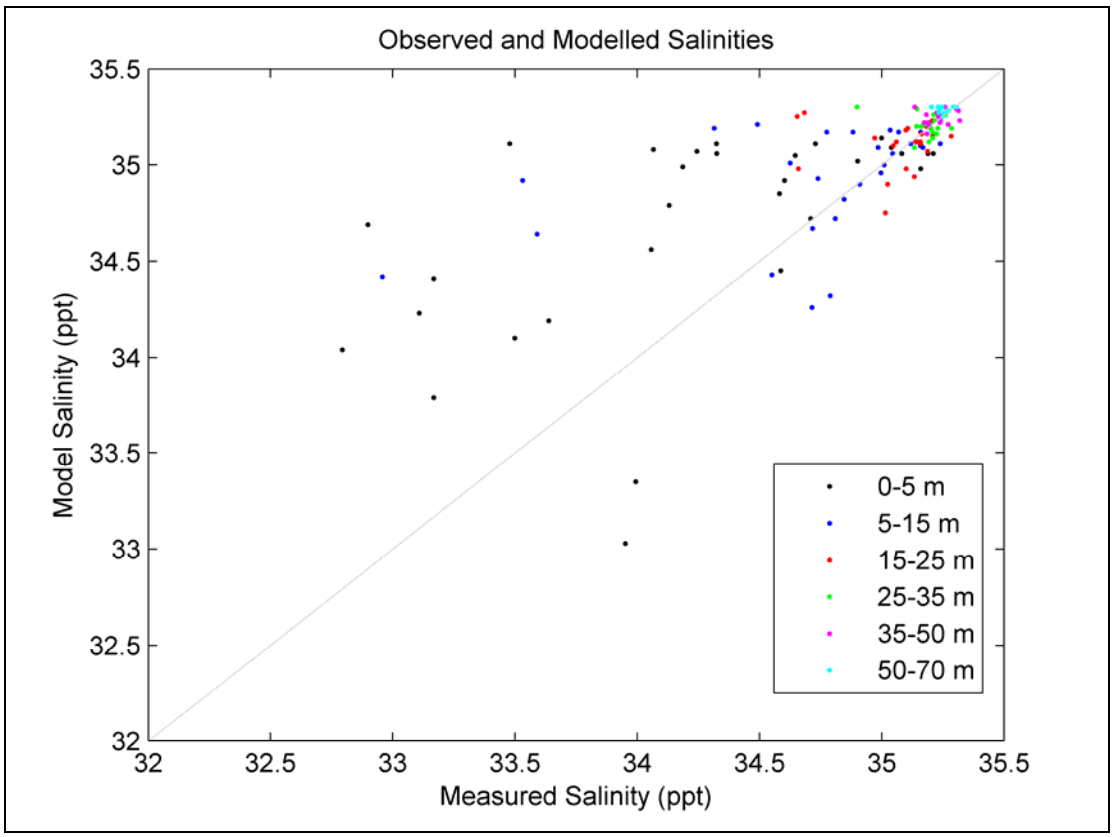

Figure 5.20 Measured and model predicted salinities during the calibration period. Measured data from CTD casts at 18 individual sites (along 3 transects), and from two time periods (17/10/2003, and 3/12/2003). Depth of salinity measurement (averaged across model layers) indicated by colour of marker.

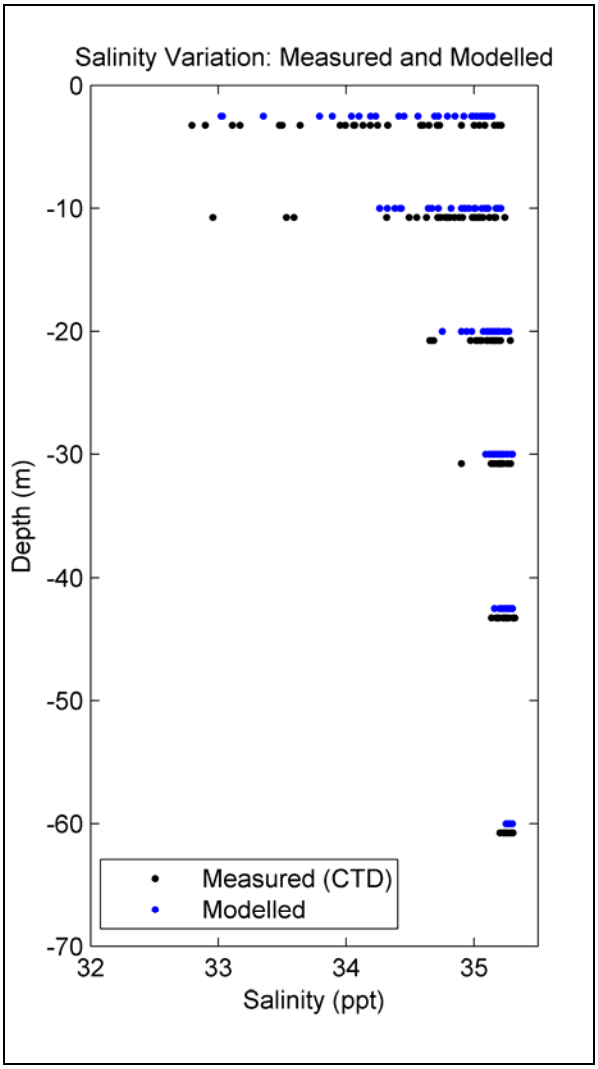

Figure 5.21 Measured (CTD) and model predicted ranges in salinity with depth from 18 individual sites within the Bay of Plenty. Measured data offset by 0.75 m vertically to aid comparisons.

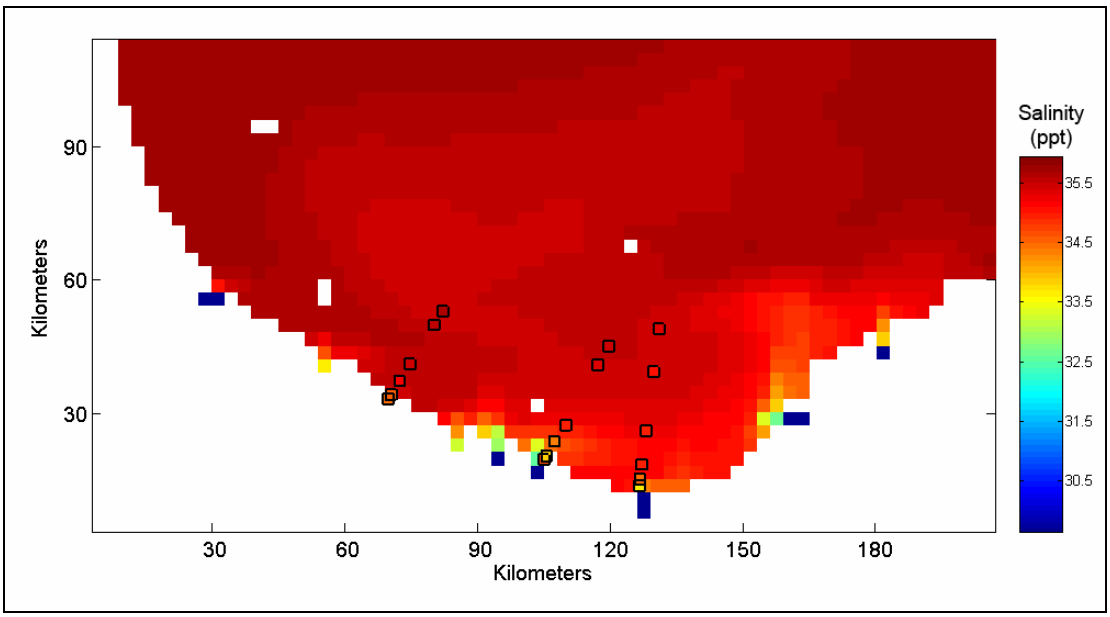

Figure 5.22 CTD measured (black squares) and model predicted salinity in the surface layer on 17/10/2003 within the Bay of Plenty.

5.7 A SEARCH FOR EXTERNAL MECHANISMS FORCING THE BAY OF PLENTY SHELF

The local wind driven hydrodynamic model replicates the circulation within the Bay of Plenty sufficiently as it stands and is adequate for the purposes of driving an ecological model as applied here. However, comparisons of the local wind driven model to both observed and inferred local wind influenced currents and sea levels highlight the potential of the Bay of Plenty to responses from external forcing mechanisms. In an effort to improve the model further, and to quantify these external forcing mechanisms and their subsequent effects on the Bay of Plenty shelf, both oceanic boundary current and coastal trapped wave influences are examined.

5.7.1 RESOLVING THE INFLUENCES OF OCEANIC BOUNDARY CURRENTS

Modelling shelf currents involves a theoretical 'separation' of the continental shelf and deep ocean. This separation, at the open boundary, creates an *Achilles heel* for shelf circulation models, as they often neglect interactions with deeper waters offshore (Huthnance, 1995; Csanady, 1997).

The EAUC (western boundary current) is known to flow southeastwards along the east coast of New Zealand's North Island (see review in Chapter 2). Whilst the majority of the EAUC flow separates and turns away from the coast at ~34^{o}S (Figures 2.4 and 2.5), a weak remnant of the original flow continues southeastward past the Bay of Plenty (Heath, 1985; Stanton *et al.*, 1997; Tilburg *et al.*, 2001). Weak southeasterly geostrophic flows (extending from oceanic regions to at least 200 m with surface speeds of ~0.14 cm.s^{-1} = 44 km.yr^{-1}) have been implied using geostrophic methods across the Bay of Plenty (Ridgeway and Grieg, 1986; Stanton *et al.*, 1997; Sutton and Chereskin, 2002). On passing the Bay of Plenty the boundary current turns East Cape and accelerates, becoming the ECC. Calculations by Stanton *et al.*, (1997) led to the conclusion that, of the water entering the ECC, only around 1 Sv (~5 % of ECC total) is sourced from flow across the greater Bay of Plenty. There is limited observational evidence, therefore, that the influence of the EAUC upon the greater Bay of Plenty is weak.

Uncertainty relating to locally specific impacts of the EAUC on the Bay of Plenty shelf, arising from a lack of focussed research in the area, leads to the necessity to incorporate a forcing mechanism replicating the EAUC into the shelf model. Accurate parameterisation of the EAUC at the open boundaries of the local wind driven model will allow the relative influences of local winds and EAUC forcing to be resolved.

5.7.1.1 THE OCCAM MODEL

The Ocean Circulation and Climate Advanced Modelling (OCCAM) project is a three-dimensional, ocean-atmosphere heat exchange, free surface global circulation model based on the ocean 'primitive' equations and solved over a 0.25^{o} grid (Webb *et al.*, 1997, 1998; Saunders *et al.*, 1999). The model is forced by winds from the European Centre for Medium-Range Weather Forecasts (ECMWF), incorporates fresh-water runoff and has 66 depth layers. Output from the OCCAM model has previously been used to force continental shelf models for the purpose of incorporating external forcing mechanisms (*e.g.* Middleton and Platov, 2003; Leth and Middleton, 2004). The reader is referred to Webb *et al.* (1997 and 1998) for further details regarding the OCCAM model initialisation, forcing, domain, boundaries, parameterisation and numerical methodologies.

Output from the OCCAM model surrounding New Zealand was obtained over 2003-2004 (co-incident with the local wind driven modelling period and data collection). These data were depth averaged and yearly means calculated (Figure 5.23). The model replicates the location of major observed flow fields surrounding New Zealand, including the EAUC and associated features, *e.g.* NCE, ECE, ECC (Figures 2.4 and 5.23). Modelled mean transport (OCCAM) in the EAUC on the southern side of the NCE is 12 Sv (September 2003 and August 2004, Figure 5.23), comparing well with observed values, 11-34 Sv (Stanton *et al.*, 1997) and ~9 Sv (Roemmich and Sutton, 1998). The larger values observed by Stanton *et al.* (1997) were attributed to temporal variability in the NCE, thought to occur over inter-annual timescales rather than seasonally (Morris *et al.*, 1996; Stanton, 2001; Stanton and Sutton, 2003).

Modelled temporal variations in the EAUC at the open boundary of the local wind-driven model cannot be directly tested due to a lack of data. However, with confidence that the OCCAM model is representing the mean aspects of the EAUC flow field adequately, and the knowledge that temporal variability is generally weak over seasonal/annual timescales (Morris *et al.*, 1996; Stanton, 2001; Stanton and Sutton, 2003), the OCCAM model output can be used to define an open boundary condition which incorporates forcing from non-locally generated effects, including the EAUC.

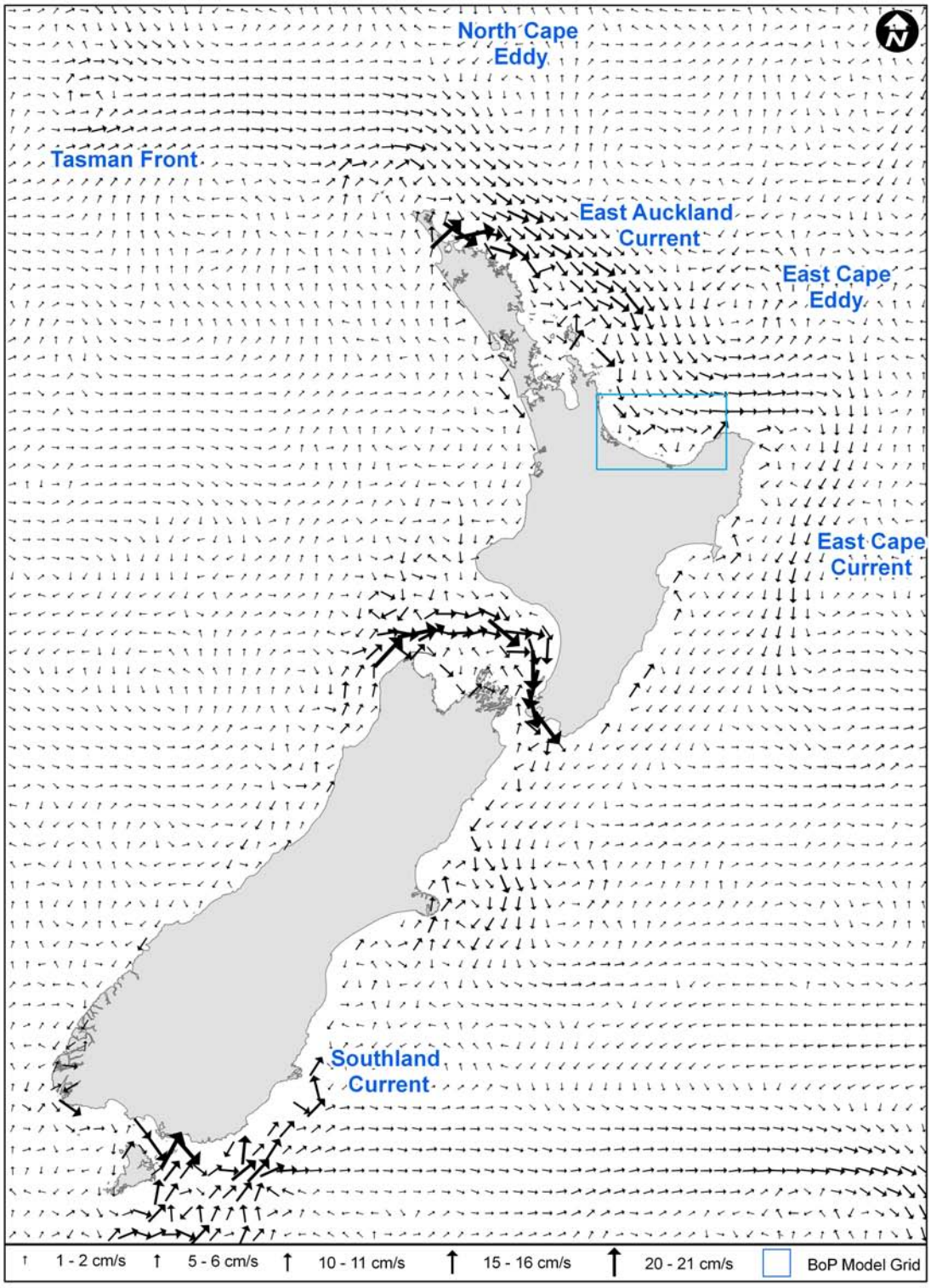

Figure 5.23 Depth averaged yearly mean flow fields surrounding New Zealand from the OCCAM model. 5-daily output averaged over the period 1 September 2003 – 31 August 2004 (time of data observations within the Bay of Plenty). Major flow features replicated by the model are named. Blue box indicates the extent of the model domain used to simulate the hydrodynamics of the Bay of Plenty shelf.

5.7.1.2 AN OCEAN CURRENT RESOLVING BOUNDARY CONDITION

Velocity profiles along the northern boundary of the local wind driven model were extracted from the OCCAM model. These profiles from the OCCAM model include velocities resulting from both local wind forcing and non-locally generated forcing mechanisms *e.g.* the EAUC. The non-locally generated forcing mechanisms are incorporated into the Bay of Plenty model by specifying these velocity profiles along the northern open boundary. Effectively the local wind-driven model is nested within the OCCAM model to incorporate externally generated influences.

5.7.1.3 A SHELF MODEL INCORPORATING BOUNDARY CURRENT FORCING

The three-dimensional baroclinic model, incorporating the OCCAM velocities along the northern open boundary, was run over the calibration interval. Other boundary conditions, initial conditions and atmospheric forcings were identical to those applied previously.

The addition of the OCCAM boundary incorporating both locally and non-locally driven currents did not improve the model's ability to predict observed currents in either a mean (Table 5.6) or fluctuating (Figures 5.24 and 5.25) sense. There are no statistically significant differences in along-shelf or cross-shelf velocities, at the Pukehina 65 m site, between the two model runs, as indicated by the Williams' T2 values (Table 5.6).

Table 5.6 Calibration coefficients of Bay of Plenty shelf hydrodynamic model, with and without OCCAM forcing, to measured data (ADP) at the Pukehina 65 m site (67 day record). All correlation coefficients significant at the 95% level. Williams' T2 statistic tests if there is a difference between two dependent correlations (Steiger, 1980), in this case values >1.96 indicate no differences between the two correlations at the 95% level.

	Model Forcing / along-shelf current correlation coefficient		Williams' T2
Model layer	Local winds	Local winds and OCCAM forcing	(Values >1.96 sig. at 95% level)
Layer 2 (5-15 m)	0.619	0.623	3.44
Layer 3 (15-25 m)	0.674	0.678	3.66
Layer 4 (25-35 m)	0.709	0.711	2.28
Layer 5 (35-50 m)	0.700	0.702	2.83

The relatively infrequent output interval of the OCCAM model (5-daily) prevents the replication of any shorter period oscillations in externally forced currents in the velocity boundary condition. However, observational evidence indicates there is little temporal variability in the EAUC over periods shorter than inter-annual timescales (Morris *et al.*, 1996; Stanton, 2001; Stanton and Sutton, 2003), meaning the 5-daily OCCAM output is temporally adequate for these modelling purposes.

With confidence that the OCCAM model replicates the EAUC flow field both in accepted direction (Figure 5.23) and magnitude (12 Sv modelled mean flows at Hauraki Gulf), a key finding is that there is no indication of systematic error due to the EAUC in the local wind driven model *i.e.* lack of representation of a consistent flow field generated by non-local forcing such as the EAUC. This suggests that the processes and forcing incorporated in the OCCAM model (*e.g.* large scale oceanic currents, EAUC) are not the cause of any lack of representation in the local wind driven model.

Given the assumptions made in this analysis we can conclude that the impact of the EAUC upon the Bay of Plenty shelf as a mean flow field is small, and that observed flow fields (which may initially appear to be extensions of the EAUC) can in fact be explained by local wind forcing. This local wind forcing can, however, force warm offshore sub-tropical water onto the Bay of Plenty shelf. The distinction is made though, that local rather than external forces drive this transport. The temperature and salinity characteristics of this sub-tropical water are incorporated into the local wind driven model through the time variable temperature and salinity boundary conditions.

This finding is consistent with conservative calculations made using geostrophic velocities through the Bay of Plenty region (Chapter 2). These calculations indicated that although between 9-34 Sv was transported in the EAUC off the Hauraki Gulf, very little (0.28 Sv) was transported offshore from the Bay of Plenty (Stanton *et al.*, 1997; Roemmich and Sutton, 1998; Chapter 2).

The lack of influence of large scale processes (as a mean flow field) which are replicated by the OCCAM model (*e.g.* EAUC) on the Bay of Plenty requires that alternate explanations be investigated in the attempt to improve the performance of the shelf model.

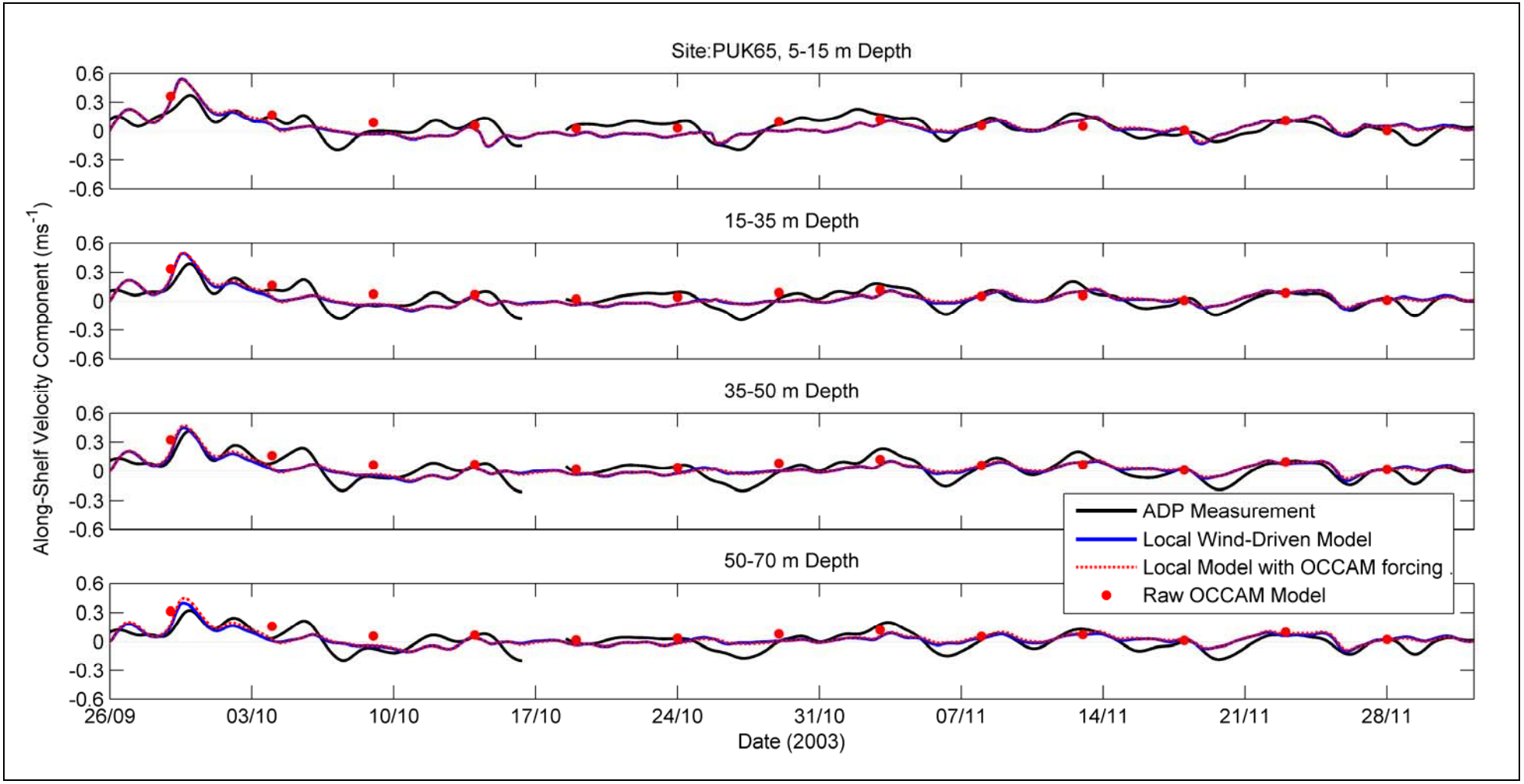

Figure 5.24 Measured (ADP) and modelled (local wind driven, local wind driven with OCCAM forcing, and direct OCCAM output) along-shelf velocities at the Pukehina 65 m site.

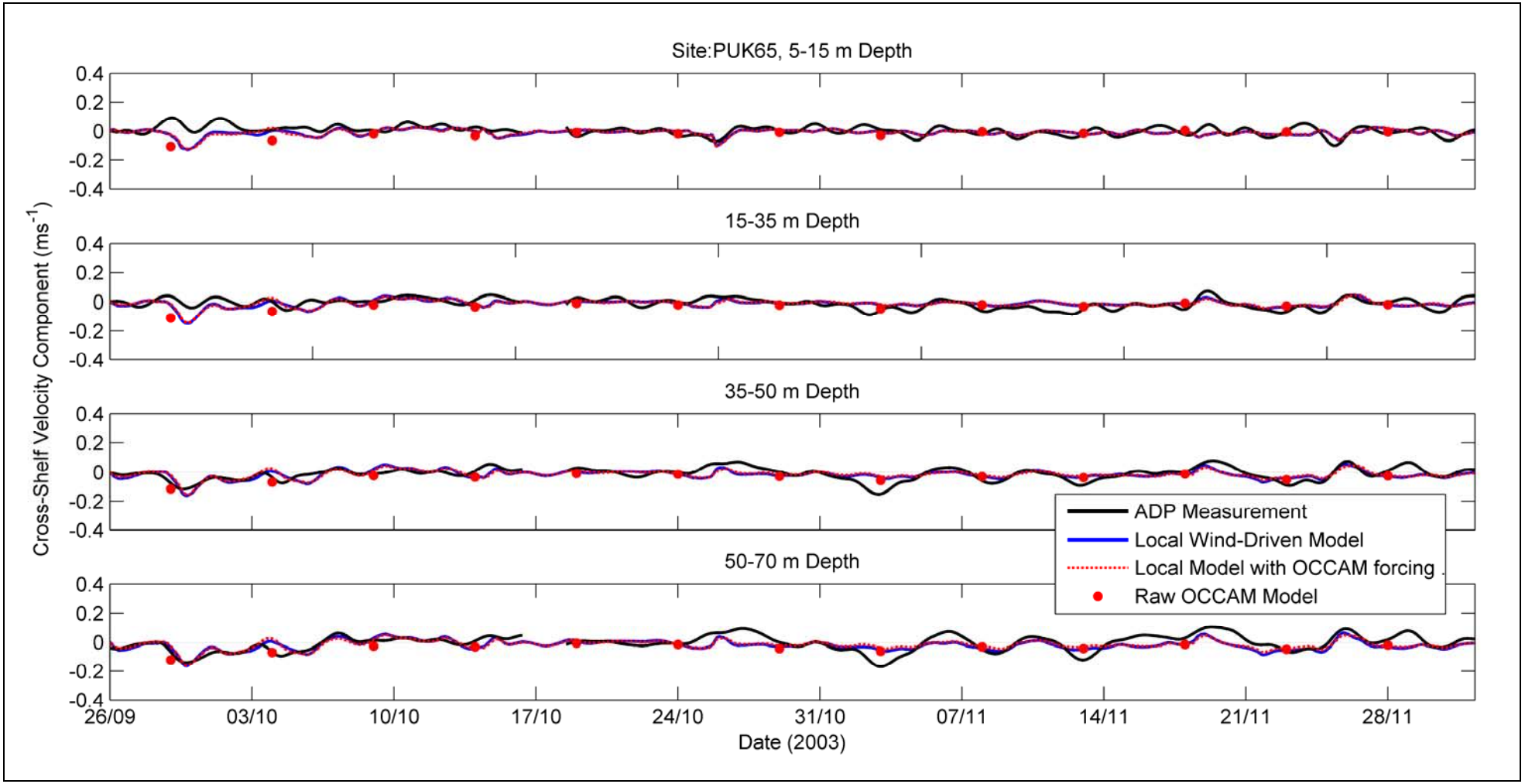

Figure 5.25 Measured (ADP) and modelled (local wind driven, local wind driven with OCCAM forcing, and direct OCCAM output) cross-shelf velocities at the Pukehina 65 m site.

5.7.2 COASTAL TRAPPED WAVE DYNAMICS WITHIN THE BAY OF PLENTY

CTWs propagate cyclonically over continental shelves at sub-inertial frequencies, can be generated by a variety of mechanisms, and result in the forcing of currents over shelf environment (Huthnance, 1995). Such mechanisms include temporal (5-20 day) or spatial variations/oscillations in along-shelf wind stress over a sloping bottom. These oscillations induce spatial/temporal variations in vorticity, which in turn generates propagating waves (Huyer, 1990; Csanady, 1997). Additionally, oscillatory coastal fluxes through straits act as a further generation mechanism (Buchwald and Kachoyan, 1987).

These propagating waves may travel beyond the region in which they were created, causing sea level changes and associated flow patterns (Huyer, 1990; Csanady, 1997). Huyer (1990) notes that CTWs waves can account for the major common characteristics of fluctuating currents over the continental shelf and upper slope. However, this proposition is qualified by the statement that '*in most regions a significant fraction of the current variance remains unexplained*' (Huyer, 1990). For example CTWs can dominate over length scales of ~1000 km along the shelf of eastern Australia due to the narrowing continuous shelf (Freeland *et al*., 1986; Buchwald and Kachoyan, 1987).

Although there are no direct observations of CTWs within the Bay of Plenty (Bell and Goring, 1996), the potential for their presence is high, given previous observations (*e.g.* characteristic velocity fluctuations at Tairua, de Lange *et al.* 2003) and the presence of potential generation features (geographical origins, Middleton, 2006) such as Cook Strait and East Cape.

A detailed explanation of and search for CTWs within the Bay of Plenty is somewhat beyond the scope of the current project (and the limitations of the available dataset). However, long-term residual sea level data from both Moturiki and Mokihanau Islands (both open coast tide gauges) can be examined for features characteristic of these waves, and a backward boundary condition applied to the model if relevant.

5.7.2.1 POTENTIAL APPLICATION TO THE MODEL

Where CTW dynamics are significant and the generation area lies outside the numerical domain, models of shelf circulation have been improved through the application of a CTW paddle boundary condition (*e.g.* Mitchum and Clarke, 1986; Middleton and Black, 1994; Evans and Middleton, 1998; Leth and Middleton, 2004; Middleton, 2006 and references therein).

The CTW information is generally applied as a backward (opposite to the direction of CTW propagation) paddle type boundary condition which simulates wind-forced CTW energy generated backward of the boundary condition (Middleton, 2006). Middleton (2006) provides a detailed, comprehensive, and mathematical explanation of the application of these backward boundary conditions.

5.7.2.2 PROPAGATION OF LOW FREQUENCY SIGNALS IN RESIDUAL SEA LEVELS

5.7.2.2.1 ANALYSES IN THE TIME DOMAIN

Freeland *et al.* (1986) identified a CTW signal and its propagation speed by cross-correlating residual sea levels from tide gauges in the along-shelf dimension. They observed lagged correlation coefficients of ~0.6-0.7, and along-shelf propagation speeds of 3.34 ms^{-1}. While phase speeds of the first mode CTW signal can vary over different shelf environments (2.63 – 16 ms^{-1}, Middleton, 2006), a similarly strong cross-correlation coefficient (*cf.* Freeland *et al.*, 1986) between Moturiki and Mokohinau Islands (see Figure 2.3 for locations) would allow the determination of phase speed and of the nature of the signal, allowing a back boundary condition for the model to be created adjacent East Cape.

Given the orientation of the two tide gauges, a CTW signal similar to that observed by Freeland *et al.* (1986) would manifest itself through a high correlation in residual sea levels, with the Mokohinau site lagging the Moturiki site (indicative of cyclonic propagation) by a time characteristic of CTW propagation velocities.

Sea level observations were de-tided, low pass filtered (recursive butterworth filter < 0.6 cpd) and corrected for the IB effect based on best fit linear regression coefficients (Table 5.7).

Table 5.7 Regression and correlation coefficients for the IB effect of atmospheric pressure on non-tidal sea levels at Moturiki and Mokohinau Islands. Regression coefficients quoted with 95% error limits. Local atmospheric pressure recorded at Tauranga Airport (Moturiki Island analysis) and at Mokohinau Island. Both correlation coefficients significant at the 95 % level.

Site	Regression coeff (mm/mb)	Correlation coefficient	Duration of data
Moturiki Island	-6.6 ± 0.04	0.77	730
Mokohinau Island	-4.6 ± 0.1	0.39	668

IB corrected sea levels were then cross-correlated to filtered local along and cross-shelf winds simultaneously. Peak lags were found at 8 hours (Mokohinau) 13 hours (Moturiki), with the winds preceding the sea level response (Table 5.8).

Table 5.8 Regression and correlation coefficients of the peak responses from multiple cross-correlation analyses of winds and IB corrected, de-tided sea levels at Moturiki and Mokohinau Islands. Local winds recorded at Tauranga Airport (Moturiki Island analysis) and Mokohinau Island. Both correlation coefficients significant at the 95 % level.

Site	Regression coeff. (along-shelf wind velocity) (mm/ms^{-1})	Regression coeff. (cross-shelf wind velocity) (mm/ms^{-1})	Correlation coefficient	Lag interval (sea levels following wind) (hrs)	Duration of data
Moturiki Island	-10.5 ± 0.3	-0.6 ± 0.2	0.58	13	718
Mokohinau Island	6.6 ± 0.2	-0.6 ± 0.2	0.42	8	668.1

At Moturiki, a positive along-shelf wind stress results in a depression of the local sea level with the peak response occurring after a 13 hour period. This can be explained by the geostrophic balance set up by the wind driven circulation dynamics (Section 5.6.2.3). However, the results from an analysis of almost 2 years of data at Mokohinau Island, cannot be explained with a similar argument. At Mokohinau Island, the result suggests that a positive (toward the SE) along-shelf wind stress results in an increase in local sea levels. This is an apparent contradiction to the theory used to explain the sea level response observed at Moturiki Island.

The response of sea levels at Moturiki requires a coastal boundary to generate the cross-shelf flow divergence and lead to depressed coastal sea levels. At Moturiki Island, this is provided by the close proximity to the Bay of Plenty coastline (~500 m), whilst Mokohinau Island is a distance of ~ 45 km (though still located on the wide continental shelf) from the main New Zealand land mass (Figure 2.3). The lack of a similar dynamic relationship between winds and sea levels at Mokohinau (*cf.* Moturiki) can be explained by this distance and the relatively small size of Mokohinau Island restricting it from acting as a coastal boundary to the wind driven circulation. Any offshore directed transport near Mokohinau Island is replaced with water from between the island and the main coast, whereas at Moturiki Island the proximity of the coastal boundary creates the cross-shelf divergence and leads to the depression of local water levels. The result suggests that Mokohinau Island is beyond the influence of the geostrophically balanced circulation observed to be set up by upwelling favourable winds in the outer Hauraki Gulf (Sharples and Greig, 1998; Zeldis *et al.*, 2004a).

A cross-correlation analysis between low pass filtered residual sea levels (de-tided, IB corrected, local wind influences removed) at both Moturiki and Mokohinau Islands identified a peak response with a 6 hour lag interval (Mokohinau following Moturiki, Figure 5.26). With a 220 km separation (along-shelf) between the Moturiki and Mokohinau Islands, this corresponds to a northwards propagation speed of ~ 10 ms^{-1}, consistent with several observed mode 1 CTW signals (Middleton, 2006).

Table 5.9 Regression and correlation coefficients at maximal lagged response of Mokohinau residual sea levels to those at Moturiki. The weak relationship (significant at 95% level) suggests that the signal which propagates from Moturiki to Mokohinau is considerably damped (response at Mokohinau is 0.28 (~ 72%) of that at Moturiki.

Regression coefficient (no units)	Correlation coefficient	Lag interval (hrs)	Duration of data
0.28± 0.03	0.14	6	668

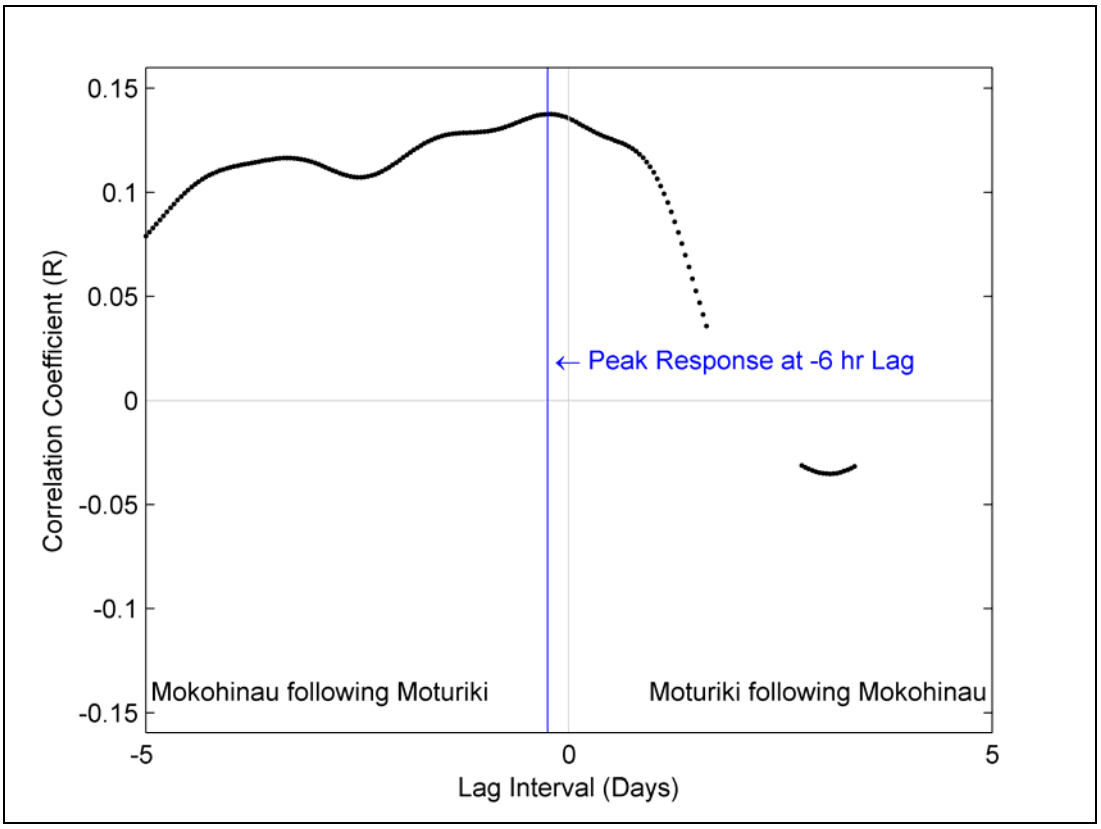

Figure 5.26 Cross-correlation coefficients of residual sea levels at Moturiki and Mokohinau Islands over a period of 668 days (1 January 2003 – 30 October 2004). Only coefficients significant at the 95% level plotted. Sea levels were low pass filtered, de-tided, corrected for the IB effect and local wind influences were removed. The peak response at a 6 hour lag suggests a propagation rate of ~10 ms^{-1} from Moturiki to Mokohinau (northward).

The relatively low correlation and regression coefficients (*cf.* Freeland *et al.*, 1986 who found coefficients of 0.6-0.7) indicate only a very weak relationship (Figure 5.26 and Table 5.9) and that the signals response at Mokohinau is severely damped (by ~70%) relative to that at Moturiki. Based solely on this evidence the response is too weak to incorporate a CTW boundary condition into the model. To complete the investigation into the presence of CTWs analyses are now carried out in the frequency domain.

5.7.2.2.2 ANALYSES IN THE FREQUENCY DOMAIN

Frequency domain analyses are popular in many attempts to resolve influences of CTWs (*e.g.* Reynaud *et al.*, 1992; Stanton, 1995) as they enable the response of forcings of different frequencies to be separated. Through a frequency domain analysis, the lag intervals of coherent signals between Moturiki and Mokohinau Islands can be identified as a function of their oscillation frequency. Should a coastal trapped wave signal be present in residual sea level data, both the dominant frequency and phase lag (and hence time lag and phase speed) can be elucidated. For a detailed summary of the methodology of the technique the reader is referred to Bell and Goring (1996) and to Emery and Thomson (2004).

Frequency domain analyses were performed on both raw and residual (de-tided, IB corrected, local wind influences removed) sea level data.

Results from the raw sea level data found, as expected, highly coherent signals at frequencies corresponding to dominant tidal constituents (Figure 5.27). At M_2 tidal frequencies, the signal was between 5-20^o out of phase, with Mokohinau lagging Moturiki. By dividing the phase shift by the specific frequency we obtain the time shift between the two signals, which indicates a time lag (at M_2 frequencies) of between 15-40 minutes.

This finding is not entirely surprising considering the established dynamics of the M_2 tide surrounding New Zealand Indeed, these results are consistent with both the direction and phase speed of this 'tidal wave' (*e.g.* Bye and Heath, 1975; Walters *et al.*, 2001; Goring and Walters 2002). The result does, however, provide confidence in the methodology, and its ability to tease out details of coherent relationships in frequency space.

Where CTWs have been identified in frequency domain analyses, either coherent peaks or consistently coherent signals were found through weather band frequencies (>~3.5 day periods, equivalent to <~0.014 cph , *e.g.* Reynaud *et al.*, 1992; Stanton, 1995). Residual sea levels at Moturiki and Mokohinau Islands are not significantly coherent at similar frequencies (Figure 5.27), suggesting there is no strong transmission of a CTW signal in sea levels between the two locations.

Coherent relationships between residual sea levels at Moturiki and Mokohinau Islands were found at frequencies corresponding to ~12.2 and ~8.0 hours, roughly corresponding to the M_2 and SK_3 tidal frequencies. While these frequencies are outside those normally associated with CTWs, it is unclear whether the result is due to some physical phenomena or a weakness in the de-tiding algorithm applied to the data.

While it remains possible a CTW signal may be present in residual water velocities (and not in sea levels) at the two sites, long-term simultaneous deployments of current meters at the two locations (minimum requirements) would be needed to identify any relationship.

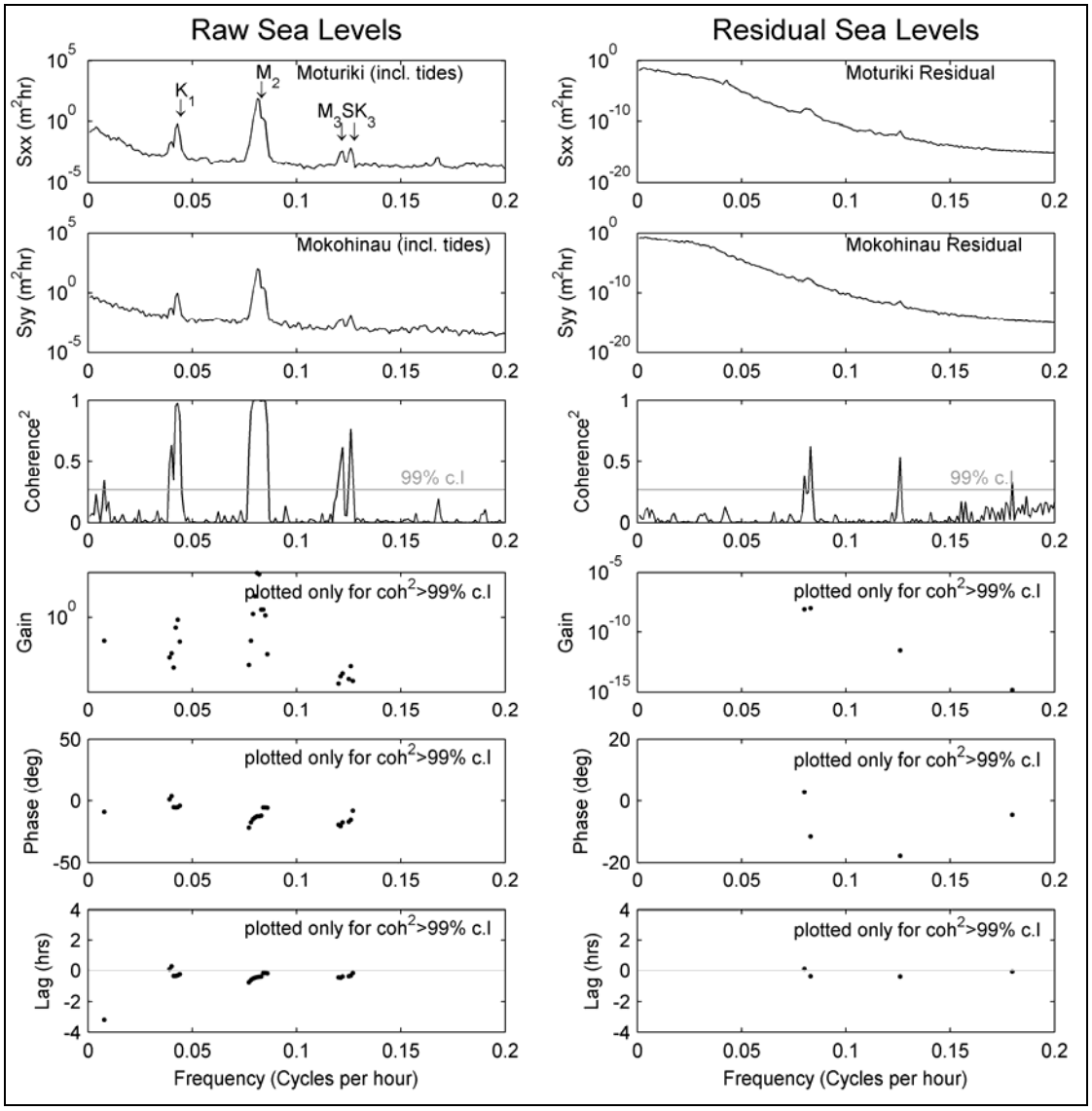

Figure 5.27 Results from analyses in the frequency domain of raw and residual (de-tided, IB corrected, wind influences removed) sea levels at Moturiki and Mokohinau Islands, showing the spectral energies and the coherence, gain and phase of the transfer function. CTW signals are typically represented by coherent signals in residual sea levels at frequencies <~ 0.014 cph. Time lag calculated by dividing the phase lag by the frequency (in deg/hr) following the methodology of Goring (1995). Negative lags indicate Mokohinau following Moturiki. Spectra were smoothed over 2 frequency intervals, yielding a confidence level of 0.26 for the squared-coherence value (99% level) (see Emery and Thomson, 2004). Values for the transfer function were only plotted where the squared-coherence exceeded this level.

5.7.2.3 COASTAL TRAPPED WAVE SIGNALS IN THE BAY OF PLENTY

Both time and frequency domain analyses of residual sea levels, from within the Bay of Plenty (Moturiki Island) and that downstream of any CTW signal (Mokohinau Island), failed to reveal any substantial evidence of CTWs within the Bay of Plenty region.

A very weak correlation was found in the time domain (R = 0.14) with a lag of 6 hours with Mokohinau following Moturiki (consistent with CTW propagation direction). When analysed as a function of the signal frequency, no significantly coherent signals were identified in the CTW frequency band between the two sites.

Based on these results there is no justification for the incorporation of at CTW paddle boundary condition to the Bay of Plenty shelf model.

5.8 SUMMARY

The hydrodynamics of the Bay of Plenty shelf have been investigated and modelled in detail. A numerical 3-dimensional wind-driven baroclinic hydrodynamic model has been calibrated ($R \approx 0.7$ for currents and $R \approx 0.8$ for sea levels) and shown to represent local velocity, sea level, salinity and temperature fields effectively. The incorporation of externally forced large scale oceanic flows did not improve the models predictive ability, implying that external forcing of the EAUC within the Bay of Plenty shelf is weak. This represents a significant finding with respect to the Bay of Plenty shelf, as the detailed dynamics of the EAUC through the region are largely unknown (Ridgeway and Grieg, 1986; Stanton *et al.*, 1997; Sutton and Chereskin, 2002).

Though there are several references as to the possibility of CTWs within the Bay of Plenty (Bell and Goring, 1996; Stephens *et al.*, 2001; de Lange *et al.*, 2003), presently, there are no detailed analyses confirming these postulations. Comprehensive analyses of sea level trends within the region have failed to find evidence suggesting the presence of CTWs within the Bay of Plenty. Accordingly, there is no justification to include them in model boundary conditions.

The calibrated model includes several novel approaches, not previously applied within New Zealand. These include the use of satellite inferred wind vectors (QuikSCAT) to represent the spatial variance in the wind field, the assimilation of SST data to the upper model layers during simulations, and the application of a time variable, thermocline replicating open boundary condition for temperatures based on seasonally specific historic CTD data and AVHRR SSTs.

Additional findings from the work include:

i. typical peak ebb and flood tide currents on the Bay of Plenty shelf range between 0.05 and 0.2 ms^{-1};

ii. non-tidal flows are substantially faster than tidally generated flows and the residual movement of the tidal component over the shelf is negligible;

iii. the size of the model domain and spatial variability of the wind field over the Bay of Plenty is such that alternate solutions to land based anemometer records must be used to effectively replicate the wind field for numerical modelling;

iv. satellite inferred QuikSCAT wind fields (Lungu, 2006) are a reasonable approximation of winds within the Bay of Plenty ($R^2 = 0.71$) and contain the spatial variability required for numerical modelling;

v. sea levels at Moturiki Island respond to atmospheric pressure at a rate of 6.6 mm/hPa, a rate lower than the 'traditional' relationship (10 mm/hPa), but consistent with other locations on New Zealand's eastern coast;

vi. residual sea levels at Moturiki Island (tides and IB effect removed) respond to the local wind field with a lag time of 13 hours in a manner consistent with observed upwelling dynamics, *i.e.* the sea level drops when upwelling occurs. This finding is somewhat novel in that previously no significant relationships had been found using co-incident (*cf.* lagged) winds and sea levels (Goring, 1995);

vii. the calibrated 3-dimensional numerical model driven by local winds and density differences replicates the general features of the observed flows adequately, and the component of the observed flows explained by local winds effectively;

viii. uncertainty in meteorological data over the large spatial scales of the model domain led to problems in determining the surface heat balance. Application of a data assimilation scheme utilising satellite inferred SSTs resolved this issue;

ix. the nesting of the local model in a regional scale model which replicates the EAUC flow field did not improve the local model's ability to replicate observed shelf currents. The inference from this is that the observed EAUC flow fields within the Bay of Plenty shelf can be explained by local forcing rather than external influences; and

x. there is no evidence in residual sea levels from Moturiki and Mokohinau Islands to suggest the transmission of significant CTW energy through the Bay of Plenty. Analyses in both time and frequency domains throughout the modelling period failed to identify significant signals characteristic of CTWs.